Cell Metabolism
Clinical and Translational Report

A clinical-stage Nrf2 activator suppresses osteoclast differentiation via the iron-ornithine axis

Graphical abstract

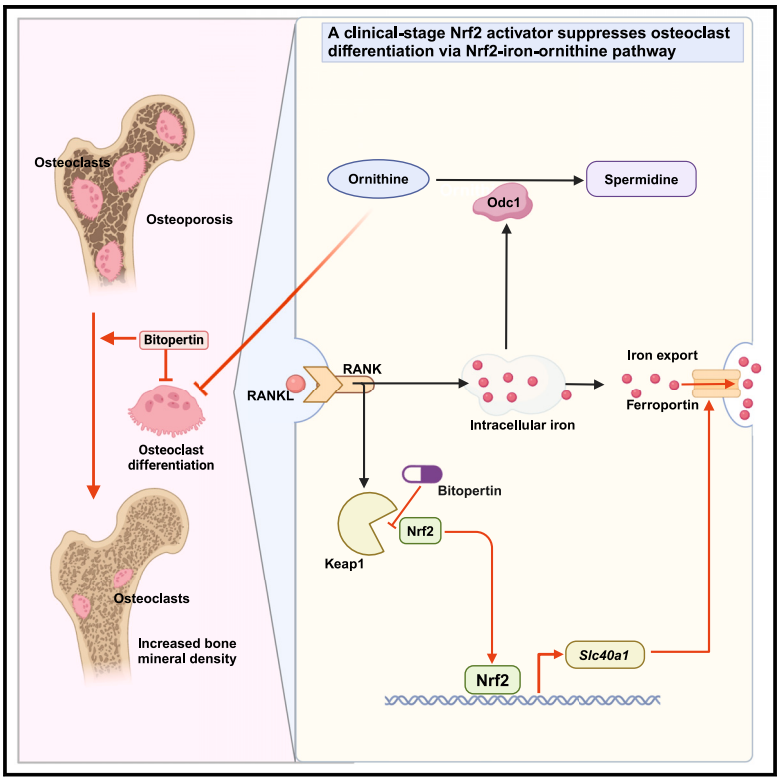

Highlights

- Bitopertin is a clinical-stage Nrf2 activator to ameliorate bone loss
- Bitopertin has fewer adverse events than clinically approved Nrf2 activators
- Nrf2 inhibits osteoclastogenesis by activating *Slc40a1* and decreasing iron levels
- Nrf2 knockout or iron supplementation reduces ornithine levels via upregulating Odc1

Authors

Yimin Dong, Honglei Kang, Renpeng Peng, ..., Xin Gan, Feng Li, Kehan Song

Correspondence

lifengmd@hust.edu.cn (F.L.), kehansong@tjh.tjmu.edu.cn (K.S.)

In brief

Dong et al. identified a clinical-stage novel Nrf2 activator that suppresses osteoclast differentiation and ameliorates estrogen-depletion-induced bone loss via a novel Nrf2-iron-ornithine pathway. In human subjects, this activator has fewer adverse events than existing clinical Nrf2 activators and may be a candidate of Nrf2 activators for clinical use.

Dong et al., 2024, Cell Metabolism *36*, 1–17
June 4, 2024
https://doi.org/10.1016/j.cmet.2024.03.005

CellPress

Please cite this article in press as: Dong et al., A clinical-stage Nrf2 activator suppresses osteoclast differentiation via the iron-ornithine axis, Cell Metabolism (2024), https://doi.org/10.1016/j.cmet.2024.03.005

Cell Metabolism

CellPress

Clinical and Translational Report

A clinical-stage Nrf2 activator suppresses osteoclast differentiation via the iron-ornithine axis

Yimin Dong,[1,4] Honglei Kang,[1,4] Renpeng Peng,[1,4] Zheming Liu,[2] Fuben Liao,[2] Shi-an Hu,[1] Weizhong Ding,[1] Pengju Wang,[1] Pengchao Yang,[1] Meipeng Zhu,[1] Sibo Wang,[1] Minglong Wu,[1] Dawei Ye,[3] Xin Gan,[1] Feng Li,[1,*] and Kehan Song[1,5,*]

[1]Department of Orthopaedic Surgery, Tongji Hospital, Tongji Medical College, Huazhong University of Science and Technology, Wuhan, China

[2]Cancer Center, Renmin Hospital of Wuhan University, Wuhan, China

[3]Cancer Center, Tongji Hospital, Tongji Medical College, Huazhong University of Science and Technology, Wuhan, China

[4]These authors contributed equally

[5]Lead contact

*Correspondence: lifengmd@hust.edu.cn (F.L.), kehansong@tjh.tjmu.edu.cn (K.S.)

https://doi.org/10.1016/j.cmet.2024.03.005

SUMMARY

Activating Nrf2 by small molecules is a promising strategy to treat postmenopausal osteoporosis. However, there is currently no Nrf2 activator approved for treating chronic diseases, and the downstream mechanism underlying the regulation of Nrf2 on osteoclast differentiation remains unclear. Here, we found that bitopertin, a clinical-stage glycine uptake inhibitor, suppresses osteoclast differentiation and ameliorates ovariectomy-induced bone loss by activating Nrf2. Mechanistically, bitopertin interacts with the Keap1 Kelch domain and decreases Keap1-Nrf2 binding, leading to reduced Nrf2 ubiquitination and degradation. Bitopertin is associated with less adverse events than clinically approved Nrf2 activators in both mice and human subjects. Furthermore, Nrf2 transcriptionally activates ferroportin-coding gene *Slc40a1* to reduce intracellular iron levels in osteoclasts. Loss of Nrf2 or iron supplementation upregulates ornithine-metabolizing enzyme Odc1, which decreases ornithine levels and thereby promotes osteoclast differentiation. Collectively, our findings identify a novel clinical-stage Nrf2 activator and propose a novel Nrf2-iron-ornithine metabolic axis in osteoclasts.

INTRODUCTION

Postmenopausal osteoporosis is a metabolic disorder caused by overactivated osteoclasts in the absence of estrogen. Decreased bone mineral density (BMD) predisposes patients to an increased risk of fragile fractures of the hip or vertebra,[1,2] causing substantial disabilities and socioeconomic burden worldwide.[3] Osteoclasts differentiate from bone-marrow-derived macrophages (BMDMs) under the stimulation of macrophage colony-stimulating factor (M-CSF) and receptor activator of nuclear factor κB ligand (RANKL). Targeting osteoclasts with bisphosphonate compounds is a mainstream strategy for the treatment of osteoporosis.[4] However, severe adverse effects and poor adherence are barriers to standardized bisphosphonate therapy in many patients, leading to undertreatment of osteoporosis.[5] Discovering novel therapeutic targets is needed to ensure better care for these patients.

Nuclear-factor-E2-related factor 2 (Nrf2) is a redox-related transcription factor, the activation of which ameliorates postmenopausal osteoporosis by suppressing osteoclast differentiation.[6] Under non-stress conditions, Nrf2 is sequestered in the cytoplasm by Keap1 and ubiquitinated by the Cul3 ubiquitin ligase for proteasome degradation.[7] During oxidative stress, Nrf2 dissociates from Keap1 and translocates to the nucleus to activate a variety of cytoprotective genes involved in cellular antioxidant responses. The Nrf2-binding sites of these genes are called antioxidant-responsive elements (AREs).[7] Because of the cytoprotective role, a number of Nrf2 activators have been discovered. However, most of them are electrophilic and indirect Nrf2 activators by covalently targeting cysteine 151 in KEAP1, and only two of them have been approved for clinical use, namely dimethyl fumarate (DMF) for treating the relapsing forms of multiple sclerosis[8] and omaveloxolone (OMA) for treating Friedreich's ataxia.[9] In addition to Keap1, these electrophilic Nrf2 activators also interact with the cysteine residues of other key enzymes or proteins and affect their function, leading to "off-target" and toxic effects.[10] In humans, indirect Nrf2 activators are associated with a high incidence rate of adverse events in clinical trials.[11] Another strategy is to find a direct inhibitor of the Keap1-Nrf2 interaction to selectively activate Nrf2.[11]

Please cite this article in press as: Dong et al., A clinical-stage Nrf2 activator suppresses osteoclast differentiation via the iron-ornithine axis, Cell Metabolism (2024), https://doi.org/10.1016/j.cmet.2024.03.005

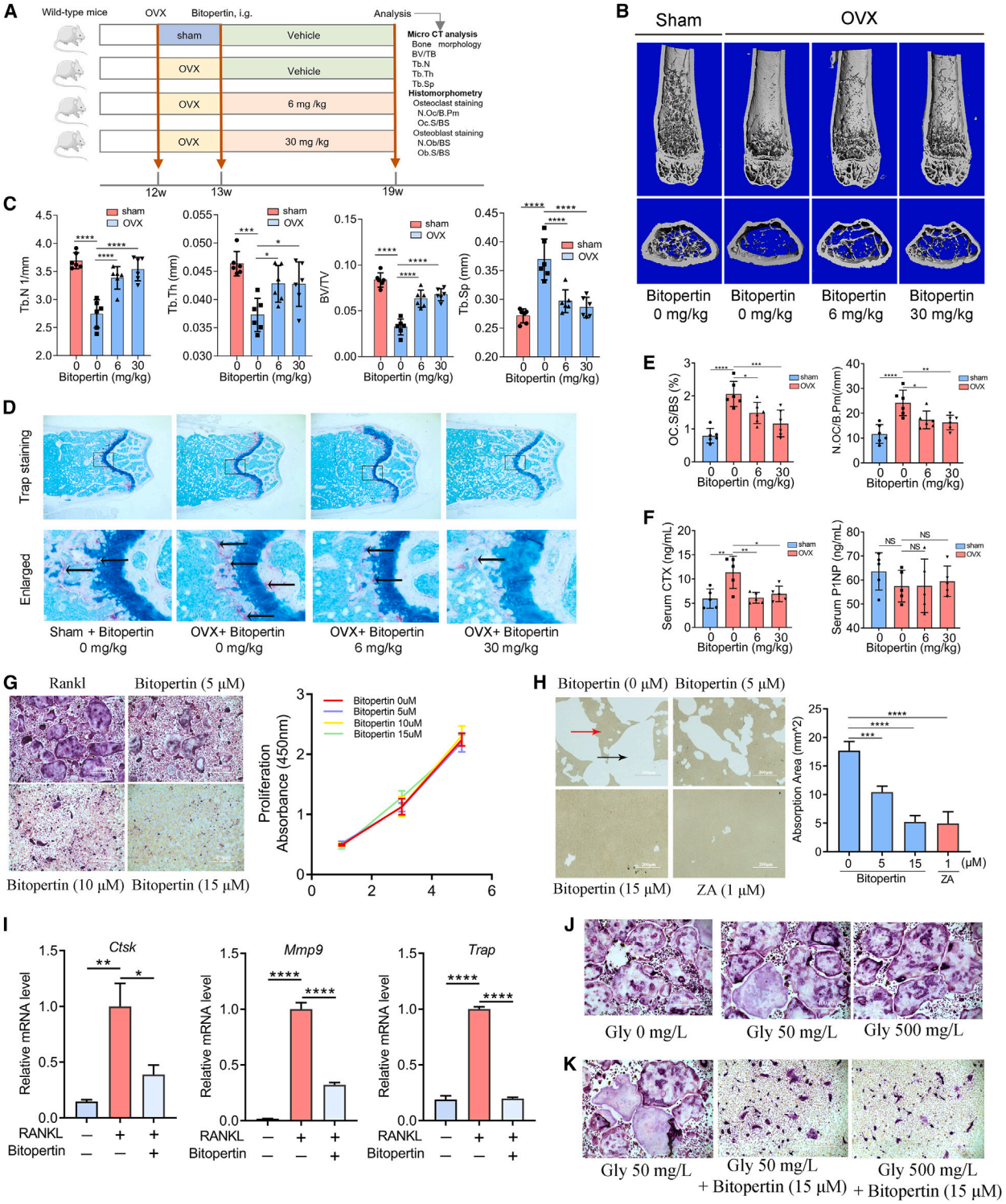

Figure 1. Bitopertin ameliorates OVX-induced osteoporosis by suppressing osteoclast formation

(A) Schematic diagram for bitopertin treatment in OVX mice.

(B) The effects of bitopertin on femur trabecular bone mass.

(C) Trabecular morphological parameters in the sham, OVX, and bitopertin-treated groups (n = 6 per group).

(D) TRAP staining of distal femur slices in each group. Black arrows indicate osteoclasts.

(E) Osteoclast-related histomorphometric parameters in each group (n = 6 in each group).

(F) Serum CTX and P1NP levels in each group (n = 5).

(legend continued on next page)

Please cite this article in press as: Dong et al., A clinical-stage Nrf2 activator suppresses osteoclast differentiation via the iron-ornithine axis, Cell Metabolism (2024), https://doi.org/10.1016/j.cmet.2024.03.005

However, direct Nrf2 activators are usually large in molecular size, which reduces their ability to enter the central nervous system to treated related diseases, and there are currently no clinically approved direct Nrf2 activators. Therefore, it remains a challenge to develop safer and more effective Nrf2 activators for clinical use.

Bitopertin is an oral, clinical glycine transporter 1 (Glyt1) inhibitor originally developed to treat schizophrenia.[12,13] Recently, bitopertin was granted orphan drug designation by the FDA for the treatment of erythropoietic protoporphyria (EPP), a rare, debilitating, and potentially life-threatening blood disorder. The efficacy of bitopertin in treating EPP is being evaluated in two ongoing phase-2 clinical trials, AURORA (NCT05308472) and BEACON (ACTRN12622000799752).[14] The potential clinical use of bitopertin is based on its role in restricting glycine uptake. Interestingly, patients with osteoporosis have significantly higher serum glycine levels than those with normal BMD.[15,16] Another study revealed that glycine supports glutathione formation and contributes to interleukin (IL)-1β production in BMDMs after LPS stimulation, indicating a pro-inflammatory role of glycine.[17] However, it remains unclear whether the elevated glycine levels are causally related to osteoporosis and whether glycine affects the differentiation of BMDMs into osteoclasts.

In this study, we ask whether blocking glycine uptake can suppress osteoclast activity and ameliorate osteoporosis. Unexpectedly, we find that bitopertin, but not glycine supplementation, ameliorates ovariectomy (OVX)-induced osteoporosis via Nrf2 activation. Mechanistically, we found that bitopertin interacts with the Kelch domain, reduces Keap1-Nrf2 interaction, and decreases Nrf2 degradation. Bitoeprtin is safer and associated with fewer adverse events in human subjects than existing clinical Nrf2 activators. More importantly, we uncovered a novel Nrf2-iron-ornithine metabolic axis in osteoclast differentiation. Our findings demonstrate a previously unrecognized therapeutic effect of bitopertin in the treatment of osteoporosis and help elucidate the molecular mechanism underlying the effects of Nrf2 on osteoclasts.

RESULTS

Bitopertin ameliorates OVX-induced osteoporosis by suppressing osteoclast formation *in vivo*

We first investigated the effect of bitopertin on the bone mass of OVX mice via oral gavage (Figure 1A). The most commonly used dose of bitopertin in previous clinical studies was 30 mg/day.[18–21] These studies did not report the body weight of the subjects. We assumed the average body weight to be 60 kg and the dose of bitopertin by body weight was 0.5 mg/kg. The equivalent dose in mice was calculated to be 6 mg/kg using the body surface area normalization method.[22] Besides, a previous animal study utilized a dose of 30 mg/kg of bitopertin.[23] Therefore, we selected 6 and 30 mg/kg of bitopertin as low and high doses, respectively, in this study.

Low and high doses of bitopertin overtly improved trabecular bone loss (Figure 1B); increased trabecular bone morphological parameters, including BV/TV, Tb.N, and Tb.Th; and decreased Tb.Sp (Figure 1C). However, cortical bone mass and morphological parameters, including Ct.Ar, Tt.Ar, Ct.Ar/Tt.Ar, and Ct.Th, were not altered (Figures S1A and S1B). TRAP staining and histomorphometry analysis showed reduced osteoclast formation and decreased N.Oc/B.Pm and Oc.S/BS in the femoral tissue after bitopertin treatment (Figures 1D and 1E). In contrast, bitopertin did not affect osteoblast formation, N.Ob/B.Pm, Ob.S/BS (Figures S1C and S1D), and mineral apposition rate of OVX mice (Figure S1E). Similarly, bitopertin decreased the serum levels of the bone resorption marker CTX but had no effect on the bone formation marker P1NP (Figure 1F). These results indicate that bitopertin ameliorates OVX-induced bone loss by suppressing osteoclast-mediated bone resorption *in vivo*.

Bitopertin suppresses osteoclast differentiation in a glycine-independent manner

In vitro, bitopertin dose-dependently suppressed osteoclast differentiation at 5–15 μM, without affecting the viability of cultured BMDMs (Figure 1G). Osteoclast resorption activity was abolished by 15 μM bitopertin, similar to the effects of 1 μM zoledronic acid (Figure 1H). In addition, the mRNA and protein expression of osteoclast-specific markers, including CTSK, MMP9, and TRAP, were downregulated by bitopertin (Figures 1I, S2A, and S2B), but the differentiation and mineralization activity of osteoblasts were not altered (Figures S2C and S2D). Similarly, the mRNA expression of osteoblast-specific genes, including *Bglap2*, *Runx2*, *Alp*, and *Col1*, was not altered by bitopertin treatment (Figure S2E).

Since bitopertin is a glycine uptake inhibitor, we then asked whether its osteoclast-suppressive effects were mediated by glycine. Interestingly, glycine deprivation or supplementation did not affect osteoclast differentiation (Figure 1J), and the inhibitory effects of bitopertin on osteoclast formation were not rescued by glycine supplementation (Figure 1K). We then knocked down the expression of the bitopertin target Glyt1 in RANKL-treated BMDMs. Western blot showed a knockdown efficacy of 70% by adeno-shRNA transfection (Figure S2F). We found that Glyt1 silencing did not affect osteoclast formation (Figure S2G). Consistent with these *in vitro* results, *in vivo* glycine administration to OVX mice did not alter trabecular bone mass (Figure S2H) and bone morphometric parameters (Figure S2I), indicating a glycine-independent role of bitopertin

(G) The effects of bitopertin on BMDM viability and osteoclast differentiation. Scale bars, 400 μM.
(H) The influence of bitopertin on osteoclastic bone resorption and the resorptive area in each group (n = 3). The red arrow indicates hydroxyapatite-coated area, and the black arrow indicates resorbed area. Scale bars, 200 μM.
(I) mRNA expression of osteoclast-related markers (n = 3) after bitopertin treatment.
(J) TRAP staining of osteoclasts cultured in glycine-deprived medium (0 mg/L), normal glycine concentration (50 mg/L), and high glycine concentration (500 mg/L) medium. Scale bars, 400 μM.
(K) Glycine supplementation on the inhibitory effects of bitopertin on osteoclast differentiation. Scale bars, 400 μM.
Data are presented as mean ± SEM. Statistical significance was determined by one-way ANOVA (C, E, F, H, and I) followed by Bonferroni multiple comparison test. Significance: *p < 0.05; **p < 0.01; ***p < 0.001; ****p < 0.0001; NS, non-significance.

Please cite this article in press as: Dong et al., A clinical-stage Nrf2 activator suppresses osteoclast differentiation via the iron-ornithine axis, Cell Metabolism (2024), https://doi.org/10.1016/j.cmet.2024.03.005

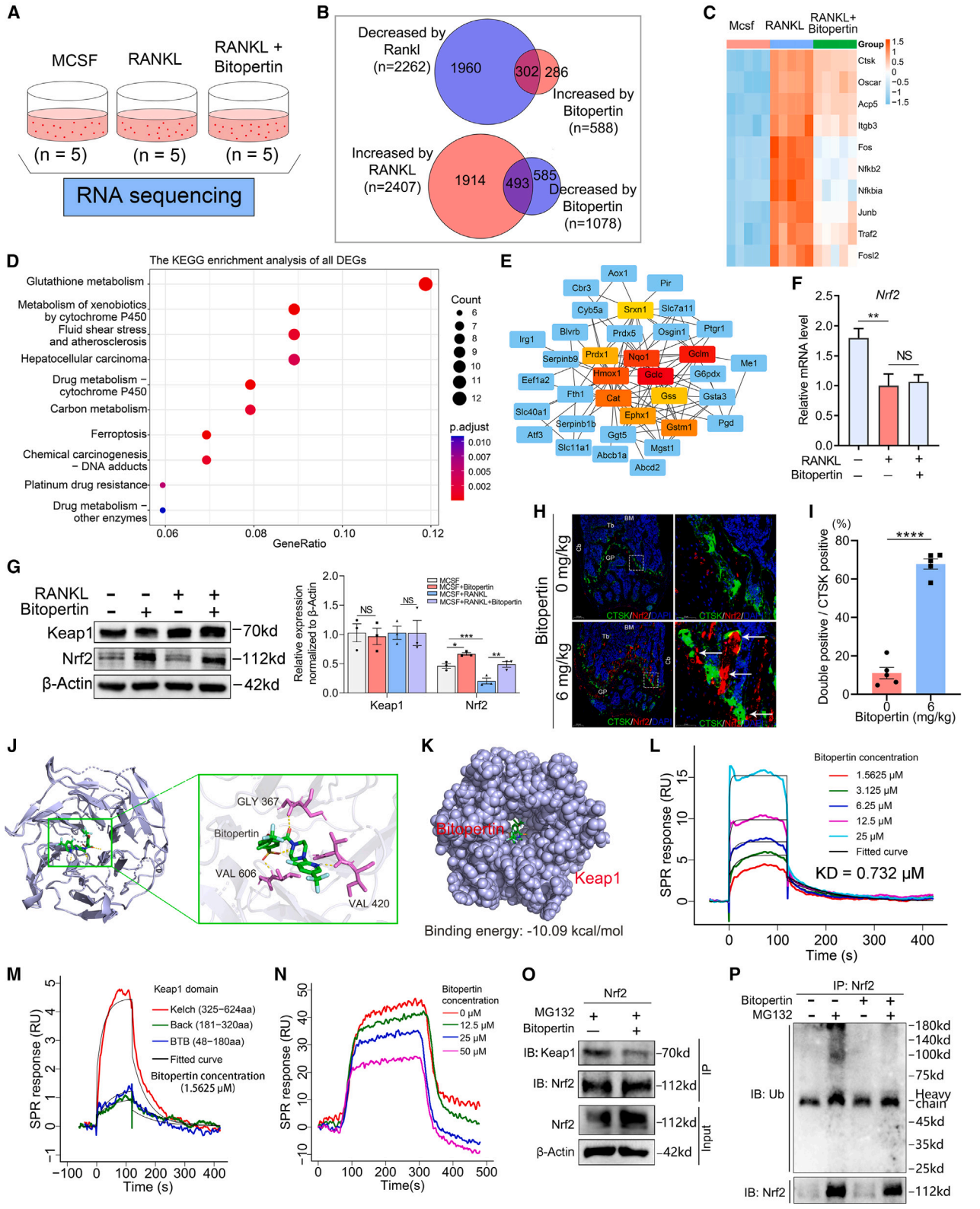

Figure 2. Bitopertin activates Nrf2 by inhibiting Keap1-Nrf2 interaction

(A) The design of the RNA sequencing assay.

(B) Differentially expressed genes among the three groups.

(legend continued on next page)

Please cite this article in press as: Dong et al., A clinical-stage Nrf2 activator suppresses osteoclast differentiation via the iron-ornithine axis, Cell Metabolism (2024), https://doi.org/10.1016/j.cmet.2024.03.005

in suppressing osteoclast differentiation and attenuating OVX-induced osteoporosis.

Bitopertin activates Nrf2 by interacting with Keap1 and suppressing Keap1-mediated Nrf2 ubiquitination

To investigate the target of bitopertin, we performed RNA sequencing (RNA-seq) on MCSF-, RANKL-, and bitopertin-treated BMDMs (Figure 2A). Principal-component analysis (PCA) revealed distinct transcriptional patterns among the three groups (Figure S3A). Using $|\log_2(\text{fold change})| > 0.5$ and $p < 0.05$, we identified 302 differentially expressed genes (DEGs) that were downregulated by RANKL but upregulated by bitopertin, and 493 DEGs that were upregulated by RANKL and downregulated by bitopertin (Figure 2B). Among the 493 DEGs, we found that RANKL-induced osteoclast-specific genes were all suppressed by bitopertin treatment (Figure 2C). Kyoto Encyclopedia of Genes and Genomes (KEGG) analysis on the 302 DEGs showed that glutathione metabolism was the most significantly enriched pathway (Figure 2D). Protein-protein interaction analysis in the STRING database followed by hub gene analysis in the Cytoscape software identified ten hub genes among the 302 DEGs, including *Gclm*, *Gclc*, *Nqo1*, *Hmox1*, *Ephx1*, *Prdx1*, *Cat*, *Gstm1*, *Gsta3*, and *Srxn1* (Figures 2E and S3B). PCR assay showed that all the ten hub genes were decreased by RANKL and increased by bitopertin treatment (Figure S3C). Immunoblotting assay showed increased expression of Gclm, Gclc, Nqo1, and Hmox1 at the protein level after bitopertin treatment (Figures S3D and S3E). Interestingly, all the ten hub genes have the ARE sequence in their promoter region and can be activated by Nrf2 (Figure S3F).[7] We reasoned that Nrf2 may be the core regulator mediating the effects of bitopertin. To validate this hypothesis, we examined the expression of Nrf2 at the mRNA and protein levels. Interestingly, the mRNA expression of Nrf2 was not changed by bitopertin treatment (Figure 2F), but the protein level was significantly increased (Figure 2G). In contrast, the expression of Keap1, the Nrf2 suppressor, was not altered by bitopertin (Figure 2G). *In vivo*, tissue immunofluorescence assay revealed increased expression of Nrf2 in the femoral trabecular bone of bitopertin-treated mice (Figure 2H). Using CTSK to label osteoclasts within the tissue, we found the ratio of CTSK and Nrf2 double-positive osteoclasts was significantly increased by bitopertin treatment (Figures 2H and 2I), indicating that Nrf2 is activated by bitopertin in osteoclasts *in vivo*.

Subsequent *in silico* molecular docking analysis was performed to investigate how bitopertin affects the Keap1-Nrf2 complex. The docking results showed that bitopertin has a high binding affinity to Keap1 by forming hydrogen bonds to the 420th and 606th valine residues and the 367th glycine residue (Figures 2J and S3G), with a binding energy of −10.09 kcal/mol (Figure 2K). The three amino acid residues are located in the Kelch domain, which directly binds to Nrf2, implying that bitopertin may disrupt Keap1-Nrf2 interaction. To validate this hypothesis, we performed surface plasmon resonance (SPR) analysis to investigate the interaction between bitopertin and Keap1. The response signal intensity between Keap1 and bitopertin in the SPR sensorgram increased with the concentration of bitopertin (Figure 2L), with a binding constant (K_D) of 0.723 μM, indicating a strong binding affinity between the two molecules. Besides, the response curve decreased after 120 s of experiment, suggesting that the binding is reversible. To further map the bitopertin binding region in Keap1, we overexpressed and purified the Kelch domain, BTB domain, and Back domains of human Keap1 protein and analyzed their binding with bitopertin. The SPR sensorgrams showed that bitopertin specifically binds to the Kelch domain of Keap1 at different concentrations (Figures 2M and S4A). The K_D value of bitopertin binding to the Kelch, BTB, and Back domain was 1.41, 1.84, and 4.16 μM, respectively (Table S4), indicating that bitopertin has a higher binding specificity to the Kelch domain than the other two domains. In a third SPR analysis, we overexpressed and purified human Keap1 and Nrf2 and investigated whether their binding could be affected by bitopertin. In the absence of bitopertin, Nrf2 showed a high affinity to Keap1, with a K_D of 0.018 μM (Table S5). However, the interaction between the two proteins was dose-dependently suppressed by bitopertin treatment (Figure 2N).

Subsequently, we performed co-immunoprecipitation and ubiquitination assays to investigate the effects of bitopertin on Keap1-Nrf2 binding in BMDMs. The results showed that Nrf2-immunoprecipitated Keap1 was diminished by bitopertin treatment (Figure 2O). The ubiquitination level of Nrf2 was decreased

(C) A heatmap showing the changes of osteoclast-specific genes among the three groups.
(D) KEGG pathway analysis of the 474 RANKL-decreased and bitopertin-activated genes.
(E) Network analysis of the hub genes among the 474 DEGs. Protein-protein interaction network was created in the STRING database, while the Cytoscape software was used to determine the hub genes in the network.
(F) The mRNA expression of Nrf2 after bitopertin treatment (n = 3).
(G) The protein expression of Nrf2 and Keap1 in BMDMs treated with bitopertin and related quantitative analysis (n = 3).
(H) Immunofluorescence of CTSK and Nrf2 in the bone marrow of distal femurs. The right panel indicates the enlarged image of the white box labeled region in the left panel. White arrows indicate the colocalization of Nrf2 and CTSK in osteoclasts in the femur tissue. Cb, cortical bone; BM, bone marrow; Tb, trabecular bone; GP, growth plate. Scale bars, 200 μM (left) and 50 μM (right).
(I) The ratio of CTSK and Nrf2 double-positive cells in CTSK-positive cells (n = 5).
(J) Molecular docking showing the binding of bitopertin to the Kelch domain of Keap1.
(K) Three-dimensional simulation and the binding energy of bitopertin and Keap1 interaction.
(L) SPR sensorgrams showing the interaction between different concentrations of bitopertin and human Keap1 protein.
(M) SPR sensorgrams showing the interaction between bitopertin and the BTB, Back, or Kelch domain of Keap1.
(N) SPR sensorgrams showing the influence of bitopertin on Nrf2 and Keap1 interaction.
(O) Co-immunoprecipitation showing the influence of bitopertin on Nrf2-Keap1 interaction in BMDMs.
(P) Nrf2 ubiquitination after bitopertin treatment.
Data are presented as mean ± SEM (F, G, and I). Statistical significance was determined by two-sided Student's t test (I), one-way ANOVA (F), or two-way ANOVA followed by Bonferroni multiple comparison test (G). Significance: *p < 0.05; **p < 0.01; ***p < 0.001; ****p < 0.0001; NS, non-significance.

Please cite this article in press as: Dong et al., A clinical-stage Nrf2 activator suppresses osteoclast differentiation via the iron-ornithine axis, Cell Metabolism (2024), https://doi.org/10.1016/j.cmet.2024.03.005

(Figure 2P), and the protein stability of Nrf2 was increased after bitopertin treatment (Figure S4B). Taken together, these data suggest that bitopertin activates Nrf2 by directly binding to the Kelch domain of Keap1 and decreases Keap1-Nrf2 interaction.

Loss of Nrf2 abolishes the effects of bitopertin on osteoclast differentiation and OVX-induced osteoporosis

We used Nrf2$^{-/-}$ mice to further validate Nrf2 as the target of bitopertin. Nrf2 knockout in BMDMs was validated at the protein level (Figure S5A). Compared with wild-type (WT) mice, Nrf2$^{-/-}$ mice showed decreased trabecular bone volume (Figure S5B); lower BV/TV, Tb.N, and Tb.Th; and higher Tb.Sp in the sham or OVX group (Figure S5C). In contrast to WT mice, bitopertin did not increase trabecular bone mass, bone parameters, and serum CTX levels in Nrf2$^{-/-}$ mice (Figures 3A–3C). Osteoclast differentiation *in vitro* was promoted and the inhibitory effects of bitopertin on osteoclasts were abolished after Nrf2 knockout (Figure 3D). Furthermore, the reduced expression of osteoclast-related proteins by bitopertin was also reversed in Nrf2$^{-/-}$ BMDMs (Figures S5D and S5E). Subsequent RNA-seq (Figure S5F) and PCA showed distinct expression patterns in the WT, WT + bitopertin, and Nrf2$^{-/-}$ + bitopertin groups (Figure S5G). Heatmap showed that Nrf2-ARE pathway genes increased by bitopertin in the WT group were all downregulated in the Nrf2$^{-/-}$ group (Figure 3E). Besides, bitopertin-induced increase of Gclc, Gclm, and Nqo1 protein expression was also abolished in Nrf2$^{-/-}$ BMDMs (Figures 3F and 3G). Gene set variation analysis (GSVA) demonstrated that bitopertin-activated glutathione metabolism, xenobiotic metabolism, and drug metabolism pathways in the previous KEGG analysis were suppressed in Nrf2$^{-/-}$ BMDMs (Figure 3H). These results suggest that the inhibitory effects of bitopertin on osteoclast differentiation and OVX-induced bone loss is mediated by Nrf2 activation.

Comparison of the safety and efficacy of bitopertin and other clinically approved Nrf2 activators in both mice and human subjects

In this part, we compared the efficacy and safety of bitopertin with the two clinically approved electrophilic Nrf2 activators, OMA (30 mg/kg) and DMF (50 mg/kg). Zoledronic acid (0.05 mg/kg) was used as positive control. After drug initiation, the mean body weight of mice in the bitopertin and DMF groups increased over time but decreased significantly in the OMA group (Figure 4A). Due to severe side effects in the OMA group, the experiment was terminated 4 weeks after treatment. Trabecular bone morphological analysis showed that DMF and bitopertin, but not OMA, prevented OVX-induced bone loss (Figure 4B). Bone morphological analysis showed that DMF and bitopertin increased BV/TV, Tb.N, and Tb.Th and decreased Tb.Sp (Figure 4C). The effects of bitopertin on trabecular bone mass and on all morphological parameters were superior to DMF and were similar to that of zoledronic acid. The three Nrf2 activators did not cause any obvious histological abnormalities in the liver, kidney, and heart tissue (Figure 4D). However, blood transaminase enzymes (alanine aminotransferase [ALT] and aspartate transaminase [AST]) were significantly increased by DMF and OMA, but not by bitopertin (Figure 4E). Serum albumin, creatine kinase, and creatine kinase (CK)-MB were not changed, and serum blood urea nitrogen (BUN) was decreased in all the three activator groups (Figures 4E–4G).

In addition to these observations in animal models, we reviewed the incidence of adverse effects associated with the Nrf2 activators in clinical trials (Table S6). We included bardoxolone, another electrophilic Nrf2 activator that has shown promising therapeutic effects for treating Alport syndrome in clinical trials but has not been approved for clinical use due to severe adverse events.[24] We found that the incidence of any adverse event or any severe adverse event associated with DMF, OMA, or bardoxolone was significantly higher than that associated with bitopertin (Figure 4H), indicating that bitopertin may be a safer candidate of Nrf2 activators for clinical use.

Nrf2 activates the transcription of the iron exporter coding gene *Slc40a1*

Although Nrf2 inhibits osteoclast differentiation, the downstream mechanism remains largely unknown.[25] We performed RNA-seq to explore the downstream molecular mechanism. WT and Nrf2$^{-/-}$ BMDMs had distinct transcriptional patterns (Figure S6A). We identified 306 downregulated and 73 upregulated DEGs in Nrf2$^{-/-}$ BMDMs, among which *Slc40a1* was the most significantly downregulated gene (Figure 5A). PCR assay showed that *Slc40a1* mRNA expression was almost completely suppressed in Nrf2$^{-/-}$ BMDMs (Figure 5B), suggesting that *Slc40a1* is regulated by Nrf2. We then investigated how Nrf2 activates *Slc40a1* transcription. The JASPAR database suggested two putative binding sites corresponding to the Nrf2-binding motif at the promoter region of human *SLC40A1* gene (Figures S6B and S6C). The first and second binding sites are located at −1,824 to −1,814 bp and −1,648 to −1,658 bp of the *SLC40A1* promote region, respectively (Figure S6D). Subsequently, we constructed luciferase reporter vectors containing the WT, binding site-1 mutant, or binding site-2 mutant promoter of *SLC40A1* gene and transfected them into 293T cells. Compared with the WT promoter group, the luciferase activity was decreased in the binding site-2 mutated group, but not in the binding site-1 mutant group (Figure 5C), suggesting that the −1,648 to −1,658 bp region of *SLC40A1* promoter is the Nrf2-binding site. Chromatin immunoprecipitation (ChIP)-qPCR analysis further validated the binding of Nrf2 to the promoter region of *SLC40A1* (Figure 5D). Subsequently, we found that the expression of *Slc40a1* was decreased by RANKL but was completely reversed by bitopertin (Figure S6E). Immunoblotting assay showed that bitopertin increased the level of ferroportin, the protein product of *Slc40a1* in WT BMDMs, but not in Nrf2$^{-/-}$ BMDMs (Figures 5E and 5F), indicating that bitopertin increases the expression of *Slc40a1* by activating Nrf2.

To further link the expression of Nrf2 and *SLC40A1* to the incidence of osteoporosis, we then analyzed the expression of *NFE2L2* (the gene encoding Nrf2) and *SLC40A1* in human osteoclast precursors using single-cell RNA-seq data of the bone tissue from patients with osteoporosis and healthy controls. We identified 16 cell populations in the two groups by uniform manifold approximation and projection (UMAP), including osteoclast and osteoblast precursors (Figure 5G). Cell ratio analysis showed higher proportion of osteoclast precursors in the osteoporosis group than the healthy control group (Figure 5H). *NFE2L2* was highly expressed in all the precursors, whereas

Please cite this article in press as: Dong et al., A clinical-stage Nrf2 activator suppresses osteoclast differentiation via the iron-ornithine axis, Cell Metabolism (2024), https://doi.org/10.1016/j.cmet.2024.03.005

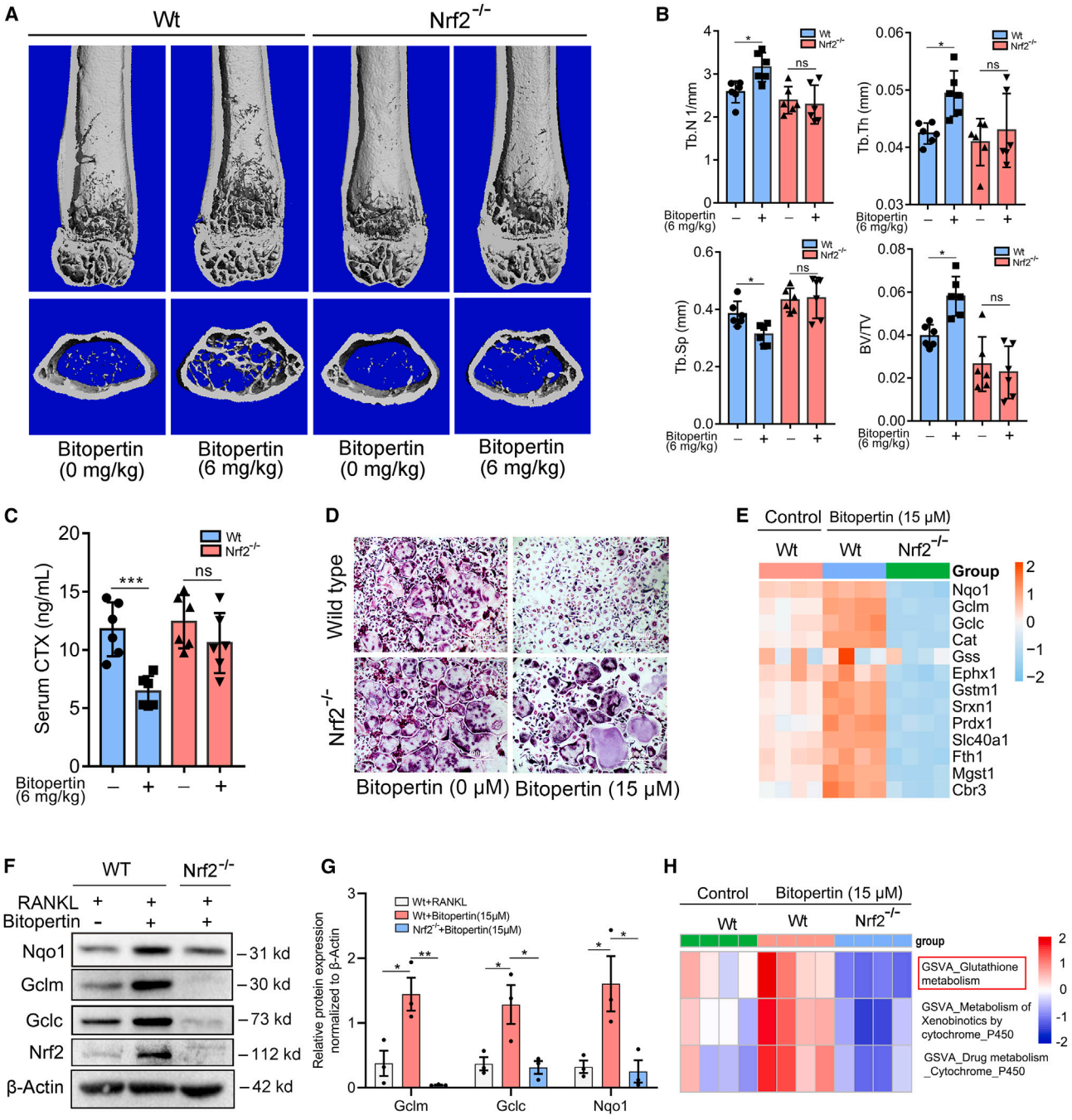

Figure 3. Loss of Nrf2 abolishes the effects of bitopertin on osteoclast differentiation and OVX-induced osteoporosis

(A) Trabecular bone mass of bitopertin-treated wild-type and Nrf2$^{-/-}$ OVX mice.

(B) Bone morphological parameters of bitopertin-treated wild-type and Nrf2$^{-/-}$ OVX mice (n = 6 per group).

(C) Serum CTX level of bitopertin-treated wild-type and Nrf2$^{-/-}$ OVX mice (n = 6 for each group).

(D) The influence of bitopertin (15 μM) on osteoclast differentiation from wild-type and Nrf2$^{-/-}$ mice. Scale bars, 400 μM.

(E) The expression of Nrf2-ARE pathway genes of bitopertin-treated wild-type and Nrf2$^{-/-}$ osteoclasts.

(F) The protein expression of Gclc, Gclm, and Nqo1 of bitopertin-treated wild-type and Nrf2$^{-/-}$ osteoclasts.

(G) Quantitative analysis of Gclc, Gclm, and Nqo1 protein expression (n = 3).

(H) Gene set variation analysis (GSVA) of the pathways in bitopertin-treated wild-type and Nrf2$^{-/-}$ osteoclasts.

Data are presented as mean ± SEM (B, C, and G). Statistical significance was determined by one-way ANOVA (G) or two-way ANOVA followed by Bonferroni multiple comparison test (B and C). Significance, *p < 0.05; **p < 0.01; ***p < 0.001; ****p < 0.0001; NS, non-significance.

Please cite this article in press as: Dong et al., A clinical-stage Nrf2 activator suppresses osteoclast differentiation via the iron-ornithine axis, Cell Metabolism (2024), https://doi.org/10.1016/j.cmet.2024.03.005

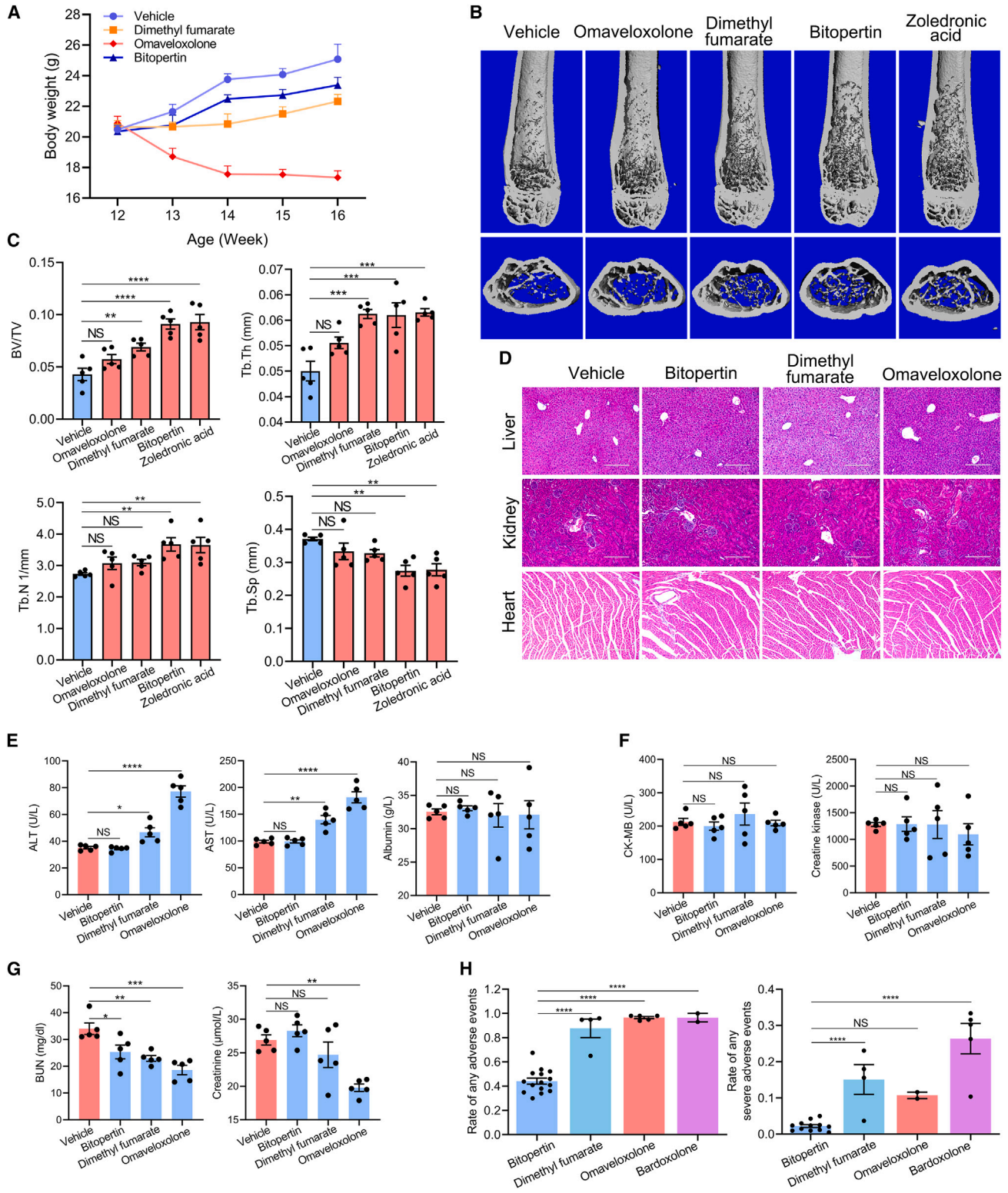

Figure 4. Comparison of bitopertin with clinically approved Nrf2 activators in mice and human subjects

(A) The body weight of OVX mice in each drug-treated group. OVX was performed at the age of 11 weeks and drug treatment was initiated at 12 weeks of age.

(B) Trabecular bone mass in each group.

(C) Bone morphological parameters in each group (n = 5).

(D) Hematoxylin and eosin staining of the liver, heart, and kidney tissue in each group. Scale bars, 400 μM.

(legend continued on next page)

Please cite this article in press as: Dong et al., A clinical-stage Nrf2 activator suppresses osteoclast differentiation via the iron-ornithine axis, Cell Metabolism (2024), https://doi.org/10.1016/j.cmet.2024.03.005

SLC40A1 was highly expressed in c-Fms^{+} macrophages (Figure 5I). In addition, the osteoporosis group showed lower proportion of *NFE2L2*-positive (Figure 5J) or *SLC40A1*-positive precursors (Figure 5K). As NRF2 promotes the transcription of *SLC40A1*, we then analyzed *SLC40A1*&NRF2 double-positive cells, and the proportion of the double-positive c-Fms^{+} macrophages was also decreased in the osteoporosis group (Figure 5L). These results indicate that the *NFE2L2-SLC40A1* axis is suppressed in osteoclast precursors of patients with osteoporosis.

Nrf2 reduces intracellular iron levels in osteoclasts via activating *Slc40a1*

Slc40a1 is the encoding gene of ferroportin, the sole iron exporter of mammalian cells. GSEA analysis of the RNA-seq data showed that the iron uptake and transport pathway was significantly changed between RANKL-treated Nrf2$^{-/-}$ and WT BMDMs (Figure 6A). In addition to *Slc40a1*, we found Nrf2$^{-/-}$ BMDMs also exhibited decreased expression of other iron-associated genes, including *Tfrc*, *Slc11a1*, and *Fth1* (Figure S6F). Intracellular iron levels were significantly increased in Nrf2$^{-/-}$ BMDMs or in RANKL-treated WT BMDMs (Figure 6B). Treatment with the Nrf2 activator bitopertin decreased intracellular iron in RANKL-treated BMDMs, but this decrease was reversed in Nrf2$^{-/-}$ BMDMs (Figure 6C). Subsequently, we knocked down the expression of *Slc40a1* by adeno-shRNA (Figure S6G) and found that *Slc40a1* silencing attenuated the iron-lowering effect of bitopertin (Figure 6D), indicating that *Slc40a1* is an essential effector of Nrf2 in regulating osteoclast iron metabolism.

Then, we investigated whether iron metabolism mediates the effects of Nrf2 on osteoclasts. Iron supplementation by ferric ammonium citrate (FAC) to the culture medium facilitated osteoclast formation (Figure 6E). In Nrf2$^{-/-}$ BMDMs, the overactivated osteoclasts were suppressed after iron chelation with deferoxamine (DFO) (Figure 6F). DFO treatment also improved bone loss (Figure 6G); increased BV/TV, Tb.N, and Tb.Th; and decreased Tb.Sp (Figure 6H) in Nrf2$^{-/-}$ OVX mice. Histomorphometric analysis revealed decreased osteoclast formation in the DFO-treated Nrf2$^{-/-}$ OVX mice (Figures S6H and S6I), whereas osteoblast formation was not changed (Figures S6J and S6K). Collectively, these results suggest that Nrf2 knockout in BMDMs increases intracellular iron level, activates osteoclast differentiation, and exacerbates bone loss in OVX models. However, chelating iron with DFO can reverse osteoclast overactivation and bone loss caused by Nrf2 knockout.

Clinical association between iron overload and the risk of osteoporosis

As iron promotes osteoclast differentiation, we then investigated the association between iron overload and osteoporosis risk. A previous genome-wide association study (GWAS) by the Genetics of Iron Status Consortium (GISC) has identified six SNPs that correlate with serum iron levels in European ancestry, including rs8177240, rs9990333, rs1800562, rs1799945, rs7385804, and rs855791.[26] In the genome sequencing data of UK Biobank participants, we found only rs1799945 was detected. rs1799945 has three genotypes, C/C, C/G, and G/G. The C allele is associated with lower serum iron levels (effect size = −0.189) in the GWAS,[26] while G is an iron-increasing allele. Another GWAS with more participants showed that the G allele of rs1799945 is associated with iron overload (transferrin saturation > 50%), with an odds ratio of 1.14.[27] We then analyzed the BMD of UK Biobank participants with different genotypes of rs1799945. As shown in Figure 6I, participants with the G allele of rs1799945 had significantly lower BMD *T* score than those with the C/C genotype, and the homozygous G/G genotype showed even lower BMD *T* scores than the heterozygous G/C genotype, suggesting that the G allele in rs1799945 also predisposes individuals to lower BMD at the individual level.

rs1799945 is located in the homeostatic iron regulator (HFE) gene, a master regulator of iron hemostasis.[28] The C to G transition of rs1799945 causes a missense mutation of the *HFE* gene, resulting in an inherited iron overload disorder called hemochromatosis.[28] We then analyzed the risk of osteoporosis associated with iron overload in a multivariate Cox regression model using the individual data from UK Biobank. We found that after adjustment for age and sex, patients with hemochromatosis had a 2.17-fold higher risk of developing osteoporosis than those without (Figure 6J). Collectively, these results suggest that excessive iron levels put individuals at higher risk of osteoporosis.

Nrf2 and iron regulate ornithine metabolism in osteoclasts

Two recent studies have suggested that both Nrf2 and iron can regulate nucleotide metabolism.[29,30] We performed metabolomics assay on DFO-treated Nrf2$^{-/-}$ BMDMs to investigate Nrf2- and iron-regulated metabolic pathways (Figure 7A). PCA suggested distinct metabolomic profiles between control and DFO-treated Nrf2$^{-/-}$ BMDMs (Figure S7A). We identified 133 downregulated and 210 upregulated metabolites after DFO treatment (Figure 7B). Metabolite KEGG analysis indicated that the arginine and proline metabolism pathway was the most significantly changed pathway (Figure 7C). The heatmap showed that most of the differential metabolites in this pathway were upregulated after DFO treatment (Figure 7D). Among these metabolites, we focused on ornithine because it is an upstream metabolite that can be metabolized into many of the other metabolites.[31] Ornithine is an intermediate amino acid produced from arginine by arginase in the urea cycle and is further metabolized to citrulline by ornithine transcarbomylase (OTC), to proline by ornithine aminotransferase (OAT), or to spermidine by ornithine decarboxylase 1 (Odc1).[31] Interestingly, the abundance of ornithine was increased, and spermidine was decreased by DFO treatment (Figure 7D). Supplementation of ornithine, but

(E) Serum alanine aminotransferase (ALT), aspartate transaminase (AST), and albumin levels in each group (n = 5).
(F) Serum creatine kinase and creatine kinase-MB (CK-MB) levels in each group (n = 5).
(G) Blood urea nitrogen (BUN) and creatinine levels in each Nrf2 activator group (n = 5).
(H) The incidence rate of any adverse event or any severe adverse event associated with bitopertin, DMF, OMA, or bardoxolone in clinical trials. See also Table S6.
Data are presented as mean ± SEM (C and E–H). Statistical significance was determined by one-way ANOVA followed by Bonferroni multiple comparison test (C and E–H). Significance: *p < 0.05; **p < 0.01; ***p < 0.001; ****p < 0.0001; NS, non-significance.

Please cite this article in press as: Dong et al., A clinical-stage Nrf2 activator suppresses osteoclast differentiation via the iron-ornithine axis, Cell Metabolism (2024), https://doi.org/10.1016/j.cmet.2024.03.005

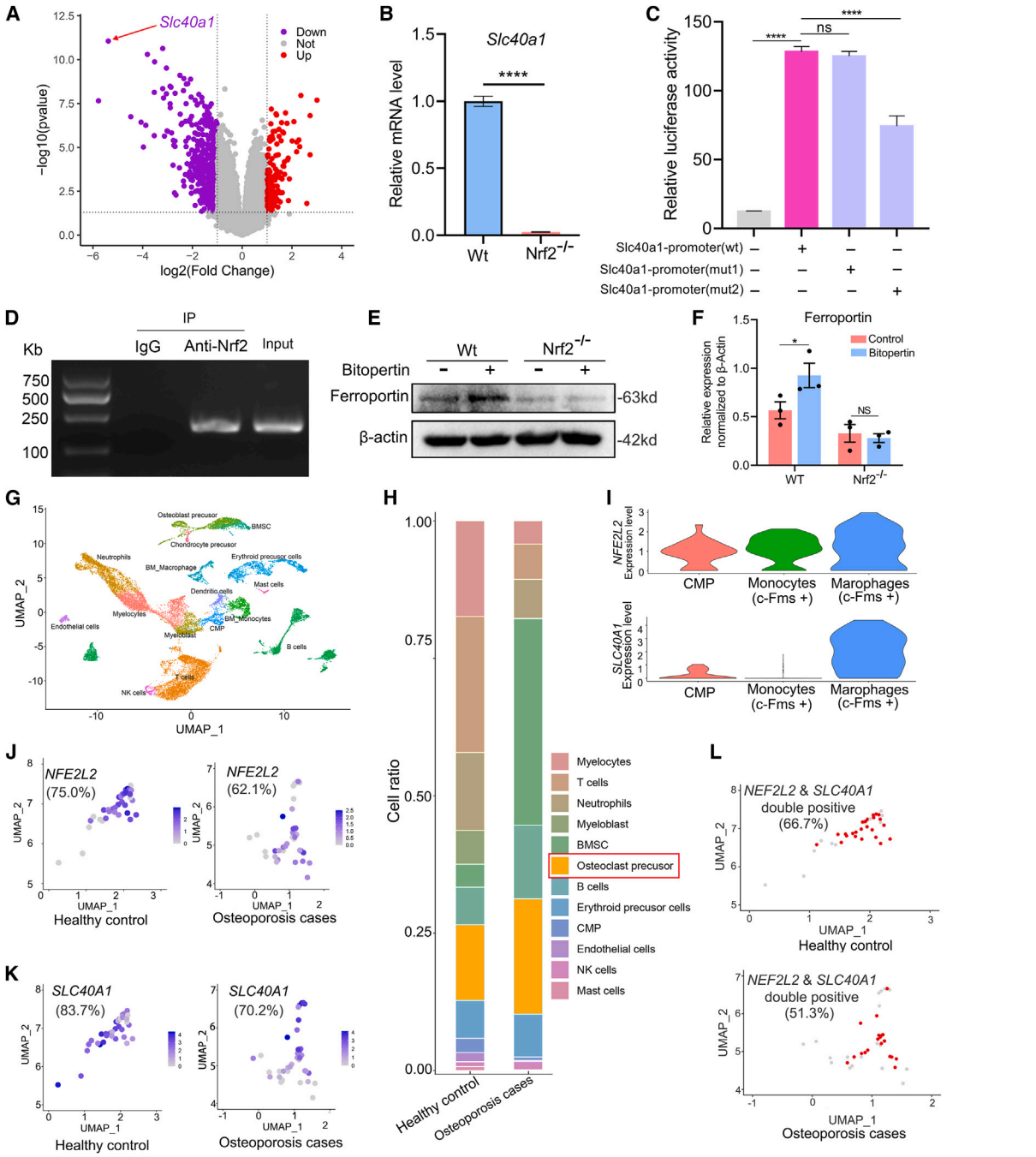

Figure 5. Nrf2 activates the transcription of the iron exporter Slc40a1

(A) Volcano plot showing differentially expressed genes between wild-type and Nrf2$^{-/-}$ BMDMs.

(B) The mRNA expression of *Slc40a1* in wild-type and Nrf2$^{-/-}$ BMDMs (n = 3 per group).

(C) Dual luciferase activity in the wild-type and mutant *SLC40A1* promoter groups (n = 3 per group).

(D) ChIP-qPCR results showing the binding of NRF2 to the promoter of *SLC40A1*. Homologous IgG antibody was used as negative control in the ChIP assay, and the input lysis was used as the positive control in the PCR analysis.

(E) The protein expression of ferroportin in bitopertin-treated wild-type and Nrf2$^{-/-}$ osteoclasts.

(F) Quantitative analysis of ferroportin protein expression (n = 3).

(G) Uniform manifold approximation and projection (UMAP) plot showing the main cell types of single-cell RNA sequencing analysis.

(H) The proportion of different cell types in the healthy controls and osteoporosis group.

(I) Relative expression of *NFE2L2* and *SLC40A1* in the myeloid linage of bone marrow cells.

(legend continued on next page)

Please cite this article in press as: Dong et al., A clinical-stage Nrf2 activator suppresses osteoclast differentiation via the iron-ornithine axis, Cell Metabolism (2024), https://doi.org/10.1016/j.cmet.2024.03.005

not spermidine, reversed the overactivation of osteoclasts from Nrf2$^{-/-}$ BMDMs (Figure S7B). In WT BMDMs, intracellular ornithine levels were increased by activating Nrf2 with bitopertin (Figure 7E). In contrast, Nrf2$^{-/-}$ BMDMs showed decreased ornithine levels (Figure 7F). However, DFO treatment significantly increased ornithine levels in Nrf2$^{-/-}$ BMDMs (Figure 7F), indicating that ornithine is a downstream metabolite regulated by Nrf2 and iron to influence osteoclast differentiation.

Subsequently, we asked how intracellular ornithine levels are regulated by Nrf2 and iron. We re-analyzed the RNA-seq data of the WT and Nrf2$^{-/-}$ BMDMs, focusing on enzymes involved in ornithine metabolism. We found that Nrf2$^{-/-}$ BMDMs showed increased expression of *Odc1*, whereas *Arg1* and *Oat* were less affected, and *Otc* was not expressed in BMDMs (Figure S7C). Supplementing iron to the culture medium increased Odc1 expression (Figure 7G). In contrast, *Odc1* expression was suppressed by the Nrf2-activator bitopertin in WT BMDMs (Figure 7H), or by the iron chelator DFO in Nrf2$^{-/-}$ BMDMs (Figure 7I). These results were consistent with the decreased spermidine abundance in the DFO-treated group (Figure 7D), suggesting that chelating iron in Nrf2$^{-/-}$ BMDMs suppresses Odc1 expression and prevents the conversion of ornithine to spermidine, leading to increased ornithine levels.

To further confirm the regulation of Nrf2 on Odc1, we treated Nrf2$^{-/-}$ BMDMs with the selective Odc1 inhibitor eflornithine and induced osteoclast differentiation. Eflornithine treatment reversed the overactivation of Nrf2$^{-/-}$ osteoclasts (Figure 7J) and reduced the mRNA levels of osteoclast markers (Figure S7D). Eflornithine treatment also decreased iron-induced osteoclast differentiation (Figure S7E). *In vivo*, eflornithine treatment improved trabecular bone loss (Figure 7K), increased bone parameters including BV/TV and Tb.N, and decreased Tb.Sp (Figure 7L) in Nrf2$^{-/-}$ OVX mice. Bone histomorphometric analysis showed decreased osteoclast formation in the femur tissue of eflornithine-treated Nrf2$^{-/-}$ OVX mice (Figures S7F and S7G), whereas osteoblast formation was not affected (Figures S7H and S7I). Collectively, these results suggest that Odc1 is regulated by Nrf2 and iron to affect ornithine metabolism, osteoclast differentiation, and bone mass.

DISCUSSION

The Keap1-Nrf2 axis responds to both oxidant and electrophile-induced stress. Nrf2 activation by small molecules is a promising strategy for the treatment of oxidative and inflammatory diseases, such as chronic kidney disease, type 2 diabetes, and neurological disorders.[32–34] Electrophilic Nrf2 activators, including clinically approved DMA and OMA, have many disadvantages, such as high incidence of adverse events and off-target effects. A novel strategy is to develop non-covalent activators that directly inhibits Keap1-Nrf2 interaction. Nevertheless, the development of such activators also faces challenges and have shortages. For example, our data indicated that Nrf2 showed a high affinity to Keap1, with a K_D value of 18 nM. To reach this K_D value, direct Nrf2 activators will be rather large in size and possess more functional groups to counteract with Nrf2 to increase their binding affinity to Keap1. The molecular weight increases as the K_D decreases.[35] Therefore, potent direct activators usually contain carboxylic acids and are too large to penetrate the blood-brain barrier, limiting their potential use in treating Nrf2-associated central nervous system diseases.[35]

In this study, we identified bitopertin as a novel clinical-stage Nrf2 activator with a K_D value of 723 nM, which is lower than that of most identified direct activators.[35,36] Although the K_D value is higher than that of Keap1-Nrf2 interaction, the Nrf2-activating effects of bitopertin were confirmed by both *in vitro* and *in vivo* results in this study. Our findings are also supported by a previous study by Matte et al.[23] They found that bitopertin has *in vivo* antioxidative effects to reduce ROS levels in circulating erythrocytes and decrease protein oxidation in the liver of β-thalassemic mice. Besides, with clinically confirmed safety and tolerability, bitopertin has superiority to existing clinically approved Nrf2 activators in terms of their effects on blood biochemistry and the incidence of adverse events associated with them. More importantly, originally designed as a Glyt1 inhibitor to treat schizophrenia, bitopertin is able to permeate the blood-brain barrier and enters the cerebrospinal fluid,[19] which can overcome the shortages of direct Keap1-Nrf2 interaction inhibitors. Conclusively, bitopertin may be a promising candidate of Nrf2 activators to treat oxidative or inflammatory diseases, particularly central nervous system diseases.

Activation of Nrf2 has been shown to inhibit osteoclast activity and ameliorate bone loss in OVX models.[37,38] The effects of Nrf2 on osteoclasts are generally thought to be mediated by suppressing ROS production, and many Nrf2 activators have been shown to inhibit osteoclast formation and bone resorption.[39,40] However, because Nrf2 activates a number of cytoprotective enzymes, it remains largely unknown which downstream effector mediates the effects of Nrf2 on osteoclasts.[25] In this study, we identified *Slc40a1* to be a direct effector of Nrf2 in osteoclasts and linked the effects of Nrf2 to cellular iron metabolism. A previous study using mouse cell lines has identified an Nrf2-binding ARE sequence outside the promoter region of mouse *Slc40a1* gene, revealing that *Slc40a1* is a target of the Nrf2-ARE signaling pathway.[41] In this study, we revealed a novel binding site of Nrf2 in the promoter region of human *SLC40A1* gene. In BMDMs from Nrf2$^{-/-}$ mice, *Slc40a1* transcription was almost abolished, leading to decrease of iron export and accumulation of intracellular iron. Our data further revealed that RANKL treatment suppressed *Slc40a1* expression, accompanied by increased iron levels in BMDMs. Excess iron can trigger ROS production via the Fenton reaction, and elevated iron has been shown to promote osteoclast differentiation.[42] We found Nrf2 activation reduced intracellular iron levels by promoting ferroportin-mediated iron export. Thus, the suppression of Nrf2 on ROS production may be, at least in part, due to decreased intracellular iron levels. These findings extend current knowledge and provide

(J and K) The proportion of *NFE2L2*-positive (J) or *SLC40A1*-positive (K) c-Fms$^+$ macrophages in each group.
(L) The proportion of *NFE2L2* and *SLC40A1* double-positive c-Fms$^+$ macrophages.
Data are presented as mean ± SEM (B, C, and F). Statistical significance was determined by two-sided Student's t test (B), one-way ANOVA (C), or two-way ANOVA followed by Bonferroni multiple comparison test (F). Significance: *p < 0.05; **p < 0.01; ***p < 0.001; ****p < 0.0001; NS, non-significance.

Please cite this article in press as: Dong et al., A clinical-stage Nrf2 activator suppresses osteoclast differentiation via the iron-ornithine axis, Cell Metabolism (2024), https://doi.org/10.1016/j.cmet.2024.03.005

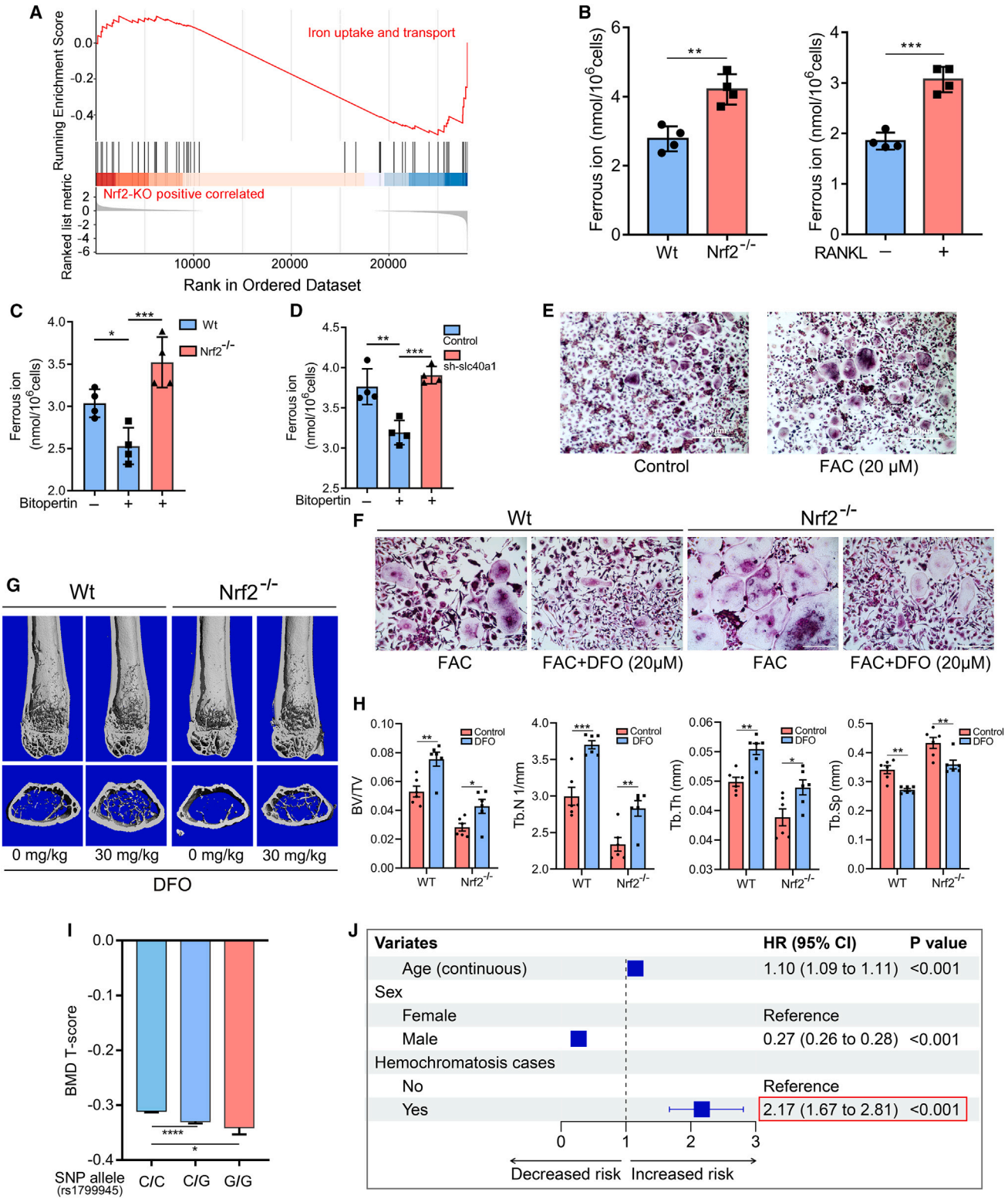

Figure 6. Nrf2 reduces intracellular iron levels in osteoclasts via activating *Slc40a1*

(A) GSEA of the iron uptake and transport pathway between the wild-type and Nrf2$^{-/-}$ group.

(B) Intracellular iron levels in wild-type and Nrf2$^{-/-}$ BMDMs and in bitopertin-treated wild-type BMDMs (n = 4 per group).

(C) Intracellular iron levels in bitopertin-treated wild-type and Nrf2$^{-/-}$ BMDMs (n = 4 per group).

(D) Intracellular iron levels in the control, bitopertin, and *Slc40a1* knockdown groups (n = 4 per group).

(legend continued on next page)

Please cite this article in press as: Dong et al., A clinical-stage Nrf2 activator suppresses osteoclast differentiation via the iron-ornithine axis, Cell Metabolism (2024), https://doi.org/10.1016/j.cmet.2024.03.005

novel insights into the effects of Nrf2 on ROS production and osteoclast differentiation.

In addition to intracellular iron control, Nrf2 have also been reported to reduce systemic iron load by activating the BMP6-hepcidin axis.[43] $Nrf2^{-/-}$ mice showed higher systemic iron load than WT mice.[43] Thus, higher iron levels in $Nrf2^{-/-}$osteoclasts may result from overloaded systemic iron. In this case, osteoclasts would have increased iron uptake via Trf1 and DMT1. However, our RNA-seq data revealed that $Nrf2^{-/-}$ osteoclasts had decreased *Tfrc* gene (encoding Tfr1) expression, and the expression of *Slc11a1* (encoding DMT1) was not altered in $Nrf2^{-/-}$ osteoclasts, indicating that $Nrf2^{-/-}$ osteoclasts are less likely to absorb more iron from the systemic pool. On the contrary, we found that the expression of *Slc40a1* (encoding ferroportin) was decreased by over 40-fold in $Nrf2^{-/-}$ osteoclasts. Dual luciferase assay and ChIP-qPCR assay evidenced that Nrf2 binds to the promoter region of *Slc40a1* gene. *In vivo* data also showed that bitopertin potently activates Nrf2 expression in osteoclasts of the femur bone marrow. These results suggest that Nrf2 suppresses osteoclast differentiation by directly regulating *Slc40a1*-mediated iron metabolism within the cells, rather than by increasing the uptake from systemic iron pool.

Two recent studies have shown that both Nrf2 and iron are regulators of nucleotide metabolism in tumor cells.[29,30] In this study, we revealed that Nrf2 and iron regulate Odc1 expression and ornithine metabolism. Odc1 is upregulated in $Nrf2^{-/-}$ cells, while the iron chelator DFO reduced Odc1 expression and increased ornithine levels in $Nrf2^{-/-}$ osteoclasts, suggesting that $Nrf2^{-/-}$ and iron control the ornithine metabolism via regulation of Odc1. An early study revealed that the Odc1 inhibitor eflornithine can suppress osteoclast differentiation from WT BMDMs.[44] In this study, we found that eflornithine suppressed the differentiation of $Nrf2^{-/-}$ osteoclasts and improved osteoclastic bone loss in $Nrf2^{-/-}$ mice. These results suggest that Odc1 is a downstream effector of Nrf2 to influence osteoclast activity and that targeting the Nrf2-iron-Odc1 axis may be a novel strategy for the treatment of osteoporosis.

There are many options to treat osteoporosis by targeting osteoclast overactivation, including bisphosphonates and denosumab, the anti-RANKL monoclonal antibody. Despite their potent anti-resorptive effects, these drugs also have drawbacks. Bisphosphonates may cause serious adverse events, including osteonecrosis of the jaw,[45] and poor patient compliance due to fear of adverse events has been reported.[5] The anti-resorptive effect of denosumab is reversible and patients are at risk of experiencing increased bone loss after drug discontinuation.[46] Activating Nrf2 is a promising strategy to suppress osteoclast differentiation and activity, and we identified bitopertin as a novel Nrf2 activator. It can improve OVX-induced bone loss by suppressing osteoclast differentiation. The safety of bitopertin has been validated in humans, and it is associated with lower rate of adverse events than other clinically approved Nrf2 activators. Therefore, bitopertin may be a good candidate for treating osteoporosis and other Nrf2-associated diseases.

Limitations of the study

This study also has some limitations. First, we identified bitopertin as a potent Nrf2 activator and revealed its therapeutic value in treating osteoporosis in mouse models, but we were unable to investigate its effects in human subjects. Second, bitopertin has been assessed in many clinical trials for treating schizophrenia, β-thalassemia, or EPP. These clinical trials were conducted based on its effects as glycine uptake inhibitor, and no clinical trial has been conducted to evaluate its efficacy as a Nrf2 activator. Future studies are needed to investigate the role of bitopertin in Nrf2-related diseases, such as chronic obstructive pulmonary disease, inflammation-related diseases. Finally, we only investigated the effects of bitopertin in OVX models, which mimic an endocrine disorder. It remains to be explored whether the Nrf2-iron-Odc1 axis also takes effect in other osteoclast-related disorders, including inflammatory bone erosion and metastatic bone diseases.

STAR★METHODS

Detailed methods are provided in the online version of this paper and include the following:

- KEY RESOURCES TABLE
- RESOURCE AVAILABILITY
  - Lead contact
  - Materials availability
  - Data and code availability
- EXPERIMENTAL MODEL AND SUBJECT DETAILS
  - UK Biobank data
  - Mouse model
  - Cell culture
- METHOD DETAILS
  - Detection of bone mineral apposition rate
  - Micro-computed tomography (μCT) analysis
  - Histomorphometry analysis
  - Immunofluorescence staining
  - Enzyme-linked immunosorbent assay (ELISA)
  - Mouse blood biochemistry assay
  - RNA sequencing and metabolomics assay
  - Bioinformatic analysis
  - Single-cell RNA-sequencing data processing and analysis
  - Molecular docking
  - Surface plasmon resonance (SPR) analysis
  - Dual luciferase reporter assay

(E) Iron supplementation (ferric ammonium citrate, 20 μM) promotes osteoclast differentiation. Scale bars, 400 μM.
(F) Deferoxamine (DFO) treatment on osteoclast differentiation in wild-type and $Nrf2^{-/-}$ mice under a high-iron (FAC, 20 μM) condition. Scale bars, 400 μM.
(G and H) Trabecular bone volume (G) and bone morphological parameters (H) of DFO-treated wild-type and $Nrf2^{-/-}$ mice (n = 6 per group).
(I) The BMD *T* score of UK Biobank participants with different rs1799945 genotypes.
(J) The risk of osteoporosis associated with hemochromatosis in multivariate Cox analysis. HR, hazard ratio; CI, confidence interval.
Data are presented as mean ± SEM (B–D, H, and I). Statistical significance was determined by two-sided Student's t test (B), one-way ANOVA (C, D, and I), or two-way ANOVA followed by Bonferroni multiple comparison test (H). Significance: *p < 0.05; **p < 0.01; ***p < 0.001; ****p < 0.0001.

Please cite this article in press as: Dong et al., A clinical-stage Nrf2 activator suppresses osteoclast differentiation via the iron-ornithine axis, Cell Metabolism (2024), https://doi.org/10.1016/j.cmet.2024.03.005

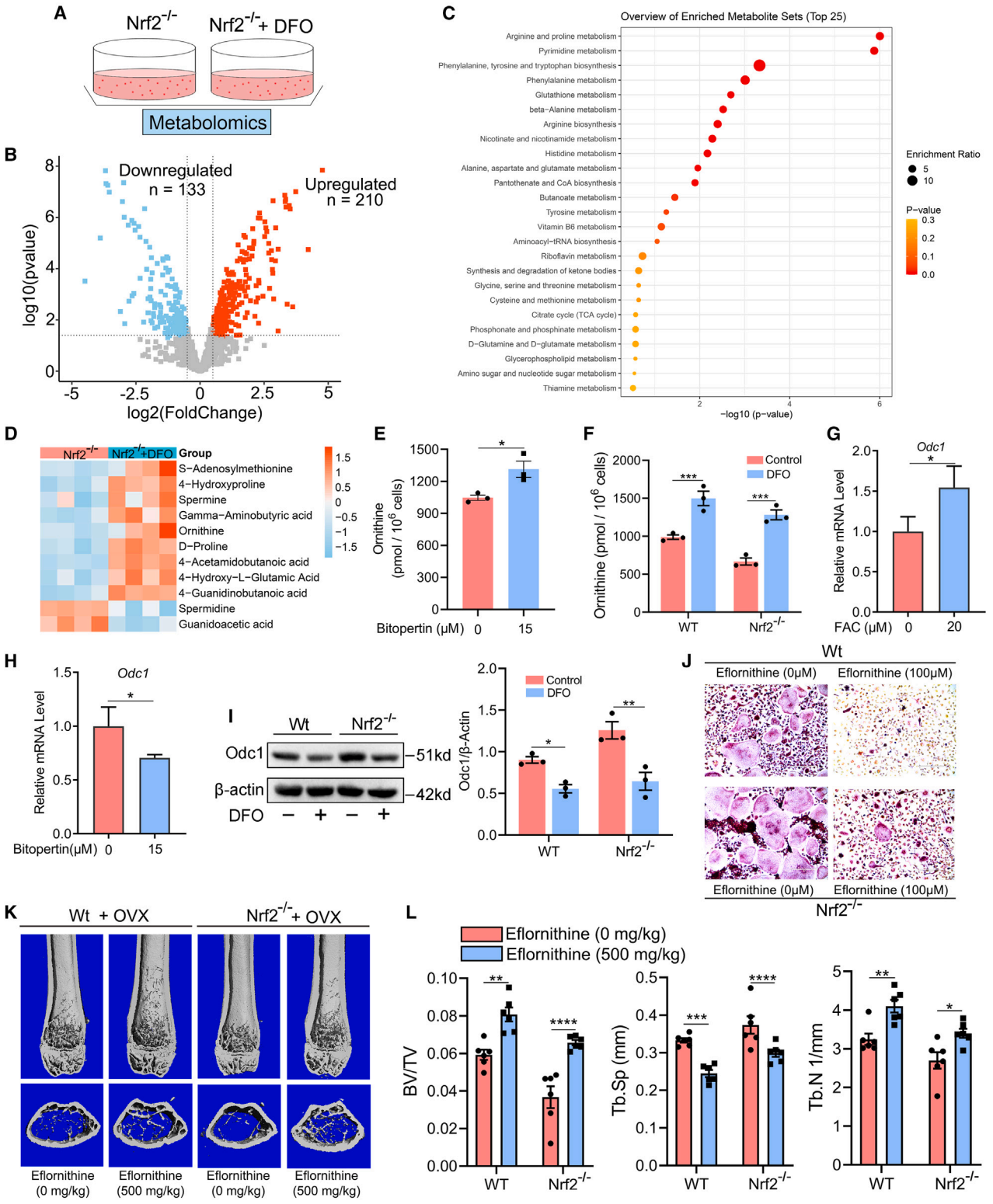

Figure 7. Nrf2 and iron regulate ornithine metabolism via Odc1

(A) A schematic diagram of the metabolomics design.

(B) Volcano plot of the differential metabolites between control and DFO-treated Nrf2$^{-/-}$ BMDMs.

(C) Metabolite KEGG pathway analysis of the differential metabolites.

(D) Changes of metabolites in the arginine and proline metabolism pathway.

(legend continued on next page)

SUPPLEMENTAL INFORMATION

Supplemental information can be found online at https://doi.org/10.1016/j.cmet.2024.03.005.

ACKNOWLEDGMENTS

This work is supported by grants from the National Natural Science Foundation of China (no. 82002354 and no. 82072500), the Key Research and Development Program of Hubei Province of China (no. 2023BCB138), and the Fundamental Research Funds for the Central Universities of China (HUST: YCJJ202201022). We thank the experts in Wuhan Yangene Biological lab, Yuechuang Center of HuaZhong Agricultural University for their generous help in the analysis and interpretation of the SPR results. The graphical abstract was generated at Biorender.com.

AUTHOR CONTRIBUTIONS

Y.D., K.S., and F.L. conceived the project. Y.D. and K.S. designed the experiments and wrote the manuscript. Y.D., H.K., R.P., and K.S. performed *in vitro* and *in vivo* studies. Y.D. performed bioinformatic analyses. Other researchers in the lab (Z.L., F.L., S.-a.H., W.D., P.W., M.Z., S.W., M.W., D.Y., and X.G.) helped with the experiments. K.S. and F.L. supervised the overall study.

DECLARATION OF INTERESTS

The authors declare no competing interests.

Received: May 16, 2023
Revised: December 14, 2023
Accepted: March 10, 2024
Published: April 2, 2024

REFERENCES

1. Dong, Y., Zhang, Y., Song, K., Kang, H., Ye, D., and Li, F. (2023). What was the epidemiology and global burden of disease of hip fractures from 1990 to 2019? Results from and additional analysis of the Global Burden of Disease Study 2019. Clin. Orthop. Relat. Res. *481*, 1209–1220. https://doi.org/10.1097/CORR.0000000000002465.
2. Dong, Y., Peng, R., Kang, H., Song, K., Guo, Q., Zhao, H., Zhu, M., Zhang, Y., Guan, H., and Li, F. (2022). Global incidence, prevalence, and disability of vertebral fractures: a systematic analysis of the global burden of disease study 2019. Spine J. *22*, 857–868. https://doi.org/10.1016/j.spinee.2021.12.007.
3. Dong, Y., Kang, H., Peng, R., Song, K., Guo, Q., Guan, H., Zhu, M., Ye, D., and Li, F. (2022). Global, regional, and national burden of low bone mineral density From 1990 to 2019: results from the Global Burden of Disease Study 2019. Front. Endocrinol. (Lausanne) *13*, 870905. https://doi.org/10.3389/fendo.2022.870905.
4. Tella, S.H., and Gallagher, J.C. (2014). Prevention and treatment of postmenopausal osteoporosis. J. Steroid Biochem. Mol. Biol. *142*, 155–170. https://doi.org/10.1016/j.jsbmb.2013.09.008.
5. Imaz, I., Zegarra, P., González-Enríquez, J., Rubio, B., Alcazar, R., and Amate, J.M. (2010). Poor bisphosphonate adherence for treatment of osteoporosis increases fracture risk: systematic review and meta-analysis. Osteoporos. Int. *21*, 1943–1951. https://doi.org/10.1007/s00198-009-1134-4.
6. Sun, Y.X., Xu, A.H., Yang, Y., and Li, J. (2015). Role of Nrf2 in bone metabolism. J. Biomed. Sci. *22*, 101. https://doi.org/10.1186/s12929-015-0212-5.
7. Shaw, P., and Chattopadhyay, A. (2020). Nrf2-ARE signaling in cellular protection: mechanism of action and the regulatory mechanisms. J. Cell. Physiol. *235*, 3119–3130. https://doi.org/10.1002/jcp.29219.
8. Blair, H.A. (2019). Dimethyl fumarate: a review in relapsing-remitting MS. Drugs *79*, 1965–1976. https://doi.org/10.1007/s40265-019-01229-3.
9. Dayalan Naidu, S., and Dinkova-Kostova, A.T. (2023). Omaveloxolone (Skyclarys™) for patients with Friedreich's ataxia. Trends Pharmacol. Sci. *44*, 394–395. https://doi.org/10.1016/j.tips.2023.03.005.
10. Dinkova-Kostova, A.T., and Copple, I.M. (2023). Advances and challenges in therapeutic targeting of NRF2. Trends Pharmacol. Sci. *44*, 137–149. https://doi.org/10.1016/j.tips.2022.12.003.
11. Abed, D.A., Goldstein, M., Albanyan, H., Jin, H., and Hu, L. (2015). Discovery of direct inhibitors of Keap1-Nrf2 protein-protein interaction as potential therapeutic and preventive agents. Acta Pharm. Sin. B *5*, 285–299. https://doi.org/10.1016/j.apsb.2015.05.008.
12. Bugarski-Kirola, D., Iwata, N., Sameljak, S., Reid, C., Blaettler, T., Millar, L., Marques, T.R., Garibaldi, G., and Kapur, S. (2016). Efficacy and safety of adjunctive bitopertin versus placebo in patients with suboptimally controlled symptoms of schizophrenia treated with antipsychotics: results from three phase 3, randomised, double-blind, parallel-group, placebo-controlled, multicentre studies in the SearchLyte clinical trial programme. Lancet Psychiatry *3*, 1115–1128. https://doi.org/10.1016/S2215-0366(16)30344-3.
13. Bugarski-Kirola, D., Blaettler, T., Arango, C., Fleischhacker, W.W., Garibaldi, G., Wang, A., Dixon, M., Bressan, R.A., Nasrallah, H., Lawrie, S., et al. (2017). Bitopertin in negative symptoms of schizophrenia-results from the phase III FlashLyte and DayLyte studies. Biol. Psychiatry *82*, 8–16. https://doi.org/10.1016/j.biopsych.2016.11.014.
14. Disc Medicine, Inc (2022). Study of bitopertin to evaluate the safety, tolerability, efficacy, and PPIX concentrations in participants with EPP. https://clinicaltrials.gov/ct2/show/NCT05308472.
15. Zhang, X., Xu, H., Li, G.H., Long, M.T., Cheung, C.L., Vasan, R.S., Hsu, Y.H., Kiel, D.P., and Liu, C.T. (2021). Metabolomics insights into osteoporosis through association with bone mineral density. J. Bone Miner. Res. *36*, 729–738. https://doi.org/10.1002/jbmr.4240.
16. Eriksson, A.L., Friedrich, N., Karlsson, M.K., Ljunggren, Ö., Lorentzon, M., Nethander, M., Wallaschofski, H., Mellström, D., and Ohlsson, C. (2021). Serum glycine levels are associated with cortical bone properties and

(E) Intracellular ornithine levels in bitopertin-treated wild-type BMDMs.
(F) Intracellular ornithine levels in DFO-treated wild-type and Nrf2$^{-/-}$ BMDMs (n = 3 per group).
(G) Iron supplementation on *Odc1* mRNA expression in wild-type BMDMs (n = 3 for each group).
(H) The effects of bitopertin on *Odc1* mRNA expression in wild-type BMDMs (n = 3 for each group).
(I) The effects of DFO on the protein level of Odc1 in wild-type and Nrf2$^{-/-}$ BMDMs and the related quantification analysis (n = 3 per group).
(J) Eflornithine suppresses osteoclast differentiation in wild-type and Nrf2$^{-/-}$ BMDMs. Scale bars, 400 μM.(K and L) The effects of eflornithine on trabecular bone mass (K) and bone morphological parameters (L) in wild-type and Nrf2$^{-/-}$ OVX mice (n = 6 per group).
Data are presented as mean ± SEM (E–I and L). Statistical significance was determined by two-sided Student's t test (E, G, and H) or two-way ANOVA followed by Bonferroni multiple comparison test (F, I, and L). Significance: *p < 0.05; **p < 0.01; ***p < 0.001; ****p < 0.0001.

fracture risk in men. J. Clin. Endocrinol. Metab. *106*, e5021–e5029. https://doi.org/10.1210/clinem/dgab544.

17. Rodriguez, A.E., Ducker, G.S., Billingham, L.K., Martinez, C.A., Mainolfi, N., Suri, V., Friedman, A., Manfredi, M.G., Weinberg, S.E., Rabinowitz, J.D., et al. (2019). Serine metabolism supports macrophage IL-1beta production. Cell Metab. *29*, 1003–1011.e4. https://doi.org/10.1016/j.cmet.2019.01.014.
18. Umbricht, D., Alberati, D., Martin-Facklam, M., Borroni, E., Youssef, E.A., Ostland, M., Wallace, T.L., Knoflach, F., Dorflinger, E., Wettstein, J.G., et al. (2014). Effect of bitopertin, a glycine reuptake inhibitor, on negative symptoms of schizophrenia: a randomized, double-blind, proof-of-concept study. JAMA Psychiatry *71*, 637–646. https://doi.org/10.1001/jamapsychiatry.2014.163.
19. Hofmann, C., Pizzagalli, F., Boetsch, C., Alberati, D., Ereshefsky, L., Jhee, S., Patat, A., Boutouyrie-Dumont, B., and Martin-Facklam, M. (2016). Effects of the glycine reuptake inhibitors bitopertin and RG7118 on glycine in cerebrospinal fluid: results of two proofs of mechanism studies in healthy volunteers. Psychopharmacol. (Berl.) *233*, 2429–2439. https://doi.org/10.1007/s00213-016-4317-7.
20. Hirayasu, Y., Sato, S.I., Shuto, N., Nakano, M., and Higuchi, T. (2017). Efficacy and safety of bitopertin in patients with schizophrenia and predominant negative symptoms: subgroup analysis of Japanese patients from the global randomized phase 2 trial. Psychiatry Investig. *14*, 63–73. https://doi.org/10.4306/pi.2017.14.1.63.
21. Taher, A.T., Viprakasit, V., Cappellini, M.D., Kraus, D., Cech, P., Volz, D., Winter, E., Nave, S., Dukart, J., Khwaja, O., et al. (2021). Haematological effects of oral administration of bitopertin, a glycine transport inhibitor, in patients with non-transfusion-dependent beta-thalassaemia. Br. J. Haematol. *194*, 474–477. https://doi.org/10.1111/bjh.17479.
22. Reagan-Shaw, S., Nihal, M., and Ahmad, N. (2008). Dose translation from animal to human studies revisited. FASEB J. *22*, 659–661. https://doi.org/10.1096/fj.07-9574LSF.
23. Matte, A., Federti, E., Winter, M., Koerner, A., Harmeier, A., Mazer, N., Tomka, T., Di Paolo, M.L., De Falco, L., Andolfo, I., et al. (2019). Bitopertin, a selective oral GLYT1 inhibitor, improves anemia in a mouse model of beta-thalassemia. JCI Insight *4*, e130111. https://doi.org/10.1172/jci.insight.130111.
24. Warady, B.A., Pergola, P.E., Agarwal, R., Andreoli, S., Appel, G.B., Bangalore, S., Block, G.A., Chapman, A.B., Chin, M.P., Gibson, K.L., et al. (2022). Effects of bardoxolone methyl in alport syndrome. Clin. J. Am. Soc. Nephrol. *17*, 1763–1774. https://doi.org/10.2215/CJN.02400222.
25. Yen, C.H., Hsu, C.M., Hsiao, S.Y., and Hsiao, H.H. (2020). Pathogenic mechanisms of myeloma bone disease and possible roles for NRF2. Int. J. Mol. Sci. *21*. https://doi.org/10.3390/ijms21186723.
26. Benyamin, B., Esko, T., Ried, J.S., Radhakrishnan, A., Vermeulen, S.H., Traglia, M., Gögele, M., Anderson, D., Broer, L., Podmore, C., et al. (2014). Novel loci affecting iron homeostasis and their effects in individuals at risk for hemochromatosis. Nat. Commun. *5*, 4926. https://doi.org/10.1038/ncomms5926.
27. Bell, S., Rigas, A.S., Magnusson, M.K., Ferkingstad, E., Allara, E., Bjornsdottir, G., Ramond, A., Sørensen, E., Halldorsson, G.H., Paul, D.S., et al. (2021). A genome-wide meta-analysis yields 46 new loci associating with biomarkers of iron homeostasis. Commun. Biol. *4*, 156. https://doi.org/10.1038/s42003-020-01575-z.
28. Papasavva, M., Vikelis, M., Katsarou, M.S., Siokas, V., Dermitzakis, E., Papademetriou, C., Karakostis, K., Lazopoulos, G., Dardiotis, E., and Drakoulis, N. (2022). Evidence that HFE H63D variant is a potential disease modifier in cluster headache. J. Mol. Neurosci. *72*, 393–400. https://doi.org/10.1007/s12031-021-01913-8.
29. Fox, D.B., Garcia, N.M.G., McKinney, B.J., Lupo, R., Noteware, L.C., Newcomb, R., Liu, J., Locasale, J.W., Hirschey, M.D., and Alvarez, J.V. (2020). NRF2 activation promotes the recurrence of dormant tumour cells through regulation of redox and nucleotide metabolism. Nat. Metab. *2*, 318–334. https://doi.org/10.1038/s42255-020-0191-z.
30. Schwartz, A.J., Goyert, J.W., Solanki, S., Kerk, S.A., Chen, B., Castillo, C., Hsu, P.P., Do, B.T., Singhal, R., Dame, M.K., et al. (2021). Hepcidin sequesters iron to sustain nucleotide metabolism and mitochondrial function in colorectal cancer epithelial cells. Nat. Metab. *3*, 969–982. https://doi.org/10.1038/s42255-021-00406-7.
31. Sivashanmugam, M., J, J., V, U., and K N, S. (2017). Ornithine and its role in metabolic diseases: an appraisal. Biomed. Pharmacother. *86*, 185–194. https://doi.org/10.1016/j.biopha.2016.12.024.
32. Pergola, P.E., Raskin, P., Toto, R.D., Meyer, C.J., Huff, J.W., Grossman, E.B., Krauth, M., Ruiz, S., Audhya, P., Christ-Schmidt, H., et al. (2011). Bardoxolone methyl and kidney function in CKD with type 2 diabetes. N. Engl. J. Med. *365*, 327–336. https://doi.org/10.1056/NEJMoa1105351.
33. Rossing, P., Block, G.A., Chin, M.P., Goldsberry, A., Heerspink, H.J.L., McCullough, P.A., Meyer, C.J., Packham, D., Pergola, P.E., Spinowitz, B., et al. (2019). Effect of bardoxolone methyl on the urine albumin-to-creatinine ratio in patients with type 2 diabetes and stage 4 chronic kidney disease. Kidney Int. *96*, 1030–1036. https://doi.org/10.1016/j.kint.2019.04.027.
34. Lynch, D.R., Chin, M.P., Delatycki, M.B., Subramony, S.H., Corti, M., Hoyle, J.C., Boesch, S., Nachbauer, W., Mariotti, C., Mathews, K.D., et al. (2021). Safety and efficacy of omaveloxolone in Friedreich ataxia (MOXIe Study). Ann. Neurol. *89*, 212–225. https://doi.org/10.1002/ana.25934.
35. Pallesen, J.S., Tran, K.T., and Bach, A. (2018). Non-covalent small-molecule kelch-like ECH-associated protein 1-nuclear factor erythroid 2-related factor 2 (Keap1-Nrf2) inhibitors and their potential for targeting central nervous system diseases. J. Med. Chem. *61*, 8088–8103. https://doi.org/10.1021/acs.jmedchem.8b00358.
36. Zhang, Y., Yan, T., Sun, D., Xie, C., Wang, T., Liu, X., Wang, J., Wang, Q., Luo, Y., Wang, P., et al. (2020). Rutaecarpine inhibits KEAP1-NRF2 interaction to activate NRF2 and ameliorate dextran sulfate sodium-induced colitis. Free Radic. Biol. Med. *148*, 33–41. https://doi.org/10.1016/j.freeradbiomed.2019.12.012.
37. Wang, J., Fang, Z., Song, C., Kang, H., Guo, Q., Dong, Y., Zhang, Y., Peng, R., Guan, H., and Li, F. (2020). Schisandrin B inhibits osteoclastogenesis and protects against ovariectomy-induced bone loss. Front. Pharmacol. *11*, 1175. https://doi.org/10.3389/fphar.2020.01175.
38. Sun, X., Xie, Z., Hu, B., Zhang, B., Ma, Y., Pan, X., Huang, H., Wang, J., Zhao, X., Jie, Z., et al. (2020). The Nrf2 activator RTA-408 attenuates osteoclastogenesis by inhibiting STING dependent NF-κB signaling. Redox Biol. *28*, 101309. https://doi.org/10.1016/j.redox.2019.101309.
39. Xu, Y., Song, D., Su, Y., Chen, J., Wu, L., Lian, H., Hai, N., Li, J., Jiang, J., Zhao, J., et al. (2023). Pharmacology-based molecular docking of 4-methylcatechol and its role in RANKL-mediated ROS/Keap1/Nrf2 signalling axis and osteoclastogenesis. Biomed. Pharmacother. *159*, 114101. https://doi.org/10.1016/j.biopha.2022.114101.
40. Xian, Y., Su, Y., Liang, J., Long, F., Feng, X., Xiao, Y., Lian, H., Xu, J., Zhao, J., Liu, Q., et al. (2021). Oroxylin A reduces osteoclast formation and bone resorption via suppressing RANKL-induced ROS and NFATc1 activation. Biochem. Pharmacol. *193*, 114761. https://doi.org/10.1016/j.bcp.2021.114761.
41. Marro, S., Chiabrando, D., Messana, E., Stolte, J., Turco, E., Tolosano, E., and Muckenthaler, M.U. (2010). Heme controls ferroportin1 (FPN1) transcription involving Bach1, Nrf2 and a MARE/ARE sequence motif at position -7007 of the FPN1 promoter. Haematologica *95*, 1261–1268. https://doi.org/10.3324/haematol.2009.020123.
42. Wang, X., Chen, B., Sun, J., Jiang, Y., Zhang, H., Zhang, P., Fei, B., and Xu, Y. (2018). Iron-induced oxidative stress stimulates osteoclast differentiation via NF-κB signaling pathway in mouse model. Metabolism *83*, 167–176. https://doi.org/10.1016/j.metabol.2018.01.005.
43. Lim, P.J., Duarte, T.L., Arezes, J., Garcia-Santos, D., Hamdi, A., Pasricha, S.R., Armitage, A.E., Mehta, H., Wideman, S., Santos, A.G., et al. (2019). Nrf2 controls iron homeostasis in haemochromatosis and thalassaemia via Bmp6 and hepcidin. Nat. Metab. *1*, 519–531. https://doi.org/10.1038/s42255-019-0063-6.

44. Lucas, R.C., Seidenfeld, J., Krieger, N.S., and Stern, P.H. (1989). Inhibition of bone resorption by alpha-difluoromethylornithine may not be mediated by polyamine depletion. J. Bone Miner. Res. *4*, 901–909. https://doi.org/10.1002/jbmr.5650040615.

45. Filleul, O., Crompot, E., and Saussez, S. (2010). Bisphosphonate-induced osteonecrosis of the jaw: a review of 2,400 patient cases. J. Cancer Res. Clin. Oncol. *136*, 1117–1124. https://doi.org/10.1007/s00432-010-0907-7.

46. Sølling, A.S., Tsourdi, E., Harsløf, T., and Langdahl, B.L. (2023). Denosumab discontinuation. Curr. Osteoporos. Rep. *21*, 95–103. https://doi.org/10.1007/s11914-022-00771-6.

47. Dong, Y., Song, K., Wang, P., Guo, J., Kang, H., Tan, X., Zhu, B., Peng, R., Zhu, M., Yu, K., et al. (2022). Blocking the cytohesin-2/ARF1 axis by SecinH3 ameliorates osteoclast-induced bone loss via attenuating JNK-mediated IRE1 endoribonuclease activity. Pharmacol. Res. *185*, 106513. https://doi.org/10.1016/j.phrs.2022.106513.

48. Frouni, I., Bédard, D., Bourgeois-Cayer, É., Hamadjida, A., Gaudette, F., Beaudry, F., and Huot, P. (2023). Pharmacokinetic profile of bitopertin, a selective $GlyT_1$ inhibitor, in the rat. Naunyn Schmiedebergs Arch. Pharmacol. *396*, 1053–1060. https://doi.org/10.1007/s00210-022-02378-1.

49. El Hafidi, M., Pérez, I., Zamora, J., Soto, V., Carvajal-Sandoval, G., and Baños, G. (2004). Glycine intake decreases plasma free fatty acids, adipose cell size, and blood pressure in sucrose-fed rats. Am. J. Physiol. Regul. Integr. Comp. Physiol. *287*, R1387–R1393. https://doi.org/10.1152/ajpregu.00159.2004.

50. Leung, S., Croft, R.J., O'Neill, B.V., and Nathan, P.J. (2008). Acute high-dose glycine attenuates mismatch negativity (MMN) in healthy human controls. Psychopharmacol. (Berl.) *196*, 451–460. https://doi.org/10.1007/s00213-007-0976-8.

51. Simmons, R.M., McKnight, S.M., Edwards, A.K., Wu, G., and Satterfield, M.C. (2020). Obesity increases hepatic glycine dehydrogenase and aminomethyltransferase expression while dietary glycine supplementation reduces white adipose tissue in Zucker diabetic fatty rats. Amino Acids *52*, 1413–1423. https://doi.org/10.1007/s00726-020-02901-9.

52. Svenningsson, A., Frisell, T., Burman, J., Salzer, J., Fink, K., Hallberg, S., Hambraeus, J., Axelsson, M., Nimer, F.A., Sundström, P., et al. (2022). Safety and efficacy of rituximab versus dimethyl fumarate in patients with relapsing-remitting multiple sclerosis or clinically isolated syndrome in Sweden: a rater-blinded, phase 3, randomised controlled trial. Lancet Neurol. *21*, 693–703. https://doi.org/10.1016/S1474-4422(22)00209-5.

53. Kang, H., Yan, Y., Jia, P., Yang, K., Guo, C., Chen, H., Qi, J., Qian, N., Xu, X., Wang, F., et al. (2016). Desferrioxamine reduces ultrahigh-molecular-weight polyethylene-induced osteolysis by restraining inflammatory osteoclastogenesis via heme oxygenase-1. Cell Death Dis. *7*, e2435. https://doi.org/10.1038/cddis.2016.339.

54. Wang, J.Y., and Johnson, L.R. (1992). Luminal polyamines substitute for tissue polyamines in duodenal mucosal repair after stress in rats. Gastroenterology *102*, 1109–1117. https://doi.org/10.1016/0016-5085(92)90745-K.

55. Dempster, D.W., Compston, J.E., Drezner, M.K., Glorieux, F.H., Kanis, J.A., Malluche, H., Meunier, P.J., Ott, S.M., Recker, R.R., and Parfitt, A.M. (2013). Standardized nomenclature, symbols, and units for bone histomorphometry: a 2012 update of the report of the ASBMR Histomorphometry Nomenclature Committee. J. Bone Miner. Res. *28*, 2–17. https://doi.org/10.1002/jbmr.1805.

56. Wang, Z., Li, X., Yang, J., Gong, Y., Zhang, H., Qiu, X., Liu, Y., Zhou, C., Chen, Y., Greenbaum, J., et al. (2021). Single-cell RNA sequencing deconvolutes the in vivo heterogeneity of human bone marrow-derived mesenchymal stem cells. Int. J. Biol. Sci. *17*, 4192–4206. https://doi.org/10.7150/ijbs.61950.

57. Qiu, X., Liu, Y., Shen, H., Wang, Z., Gong, Y., Yang, J., Li, X., Zhang, H., Chen, Y., Zhou, C., et al. (2021). Single-cell RNA sequencing of human femoral head in vivo. Aging (Albany, N.Y.) *13*, 15595–15619. https://doi.org/10.18632/aging.203124.

Please cite this article in press as: Dong et al., A clinical-stage Nrf2 activator suppresses osteoclast differentiation via the iron-ornithine axis, Cell Metabolism (2024), https://doi.org/10.1016/j.cmet.2024.03.005

STAR★METHODS

KEY RESOURCES TABLE

REAGENT or RESOURCE	SOURCE	IDENTIFIER
Antibodies		
Anti- CTSK antibody (for IF)	Santa Cruz	Cat# sc-48353; RRID:AB_2087687
Anti-CTSK antibody (for WB)	Abcam	Cat# ab207086; RRID:AB_2885178
Anti-TRAP antibody	Abcam	Cat# ab96372; RRID:AB_10679130
Anti-Glyt1 antibody	Abcam	Cat# ab113823; RRID:AB_10890812
Anti-MMP9 antibody	Proteintech	Cat# 10375-2-AP; RRID:AB_10897178
Anti- ubiquitin antibody	Proteintech	Cat# 10201-2-AP; RRID:AB_671515
Anti-Nrf2 antibody	Proteintech	Cat# 16396-1-AP; RRID:AB_2782956
Anti-Keap1 antibody	Proteintech	Cat# 10503-2-AP; RRID:AB_2132625
Anti-HO1 antibody	Proteintech	Cat# 10701-1-AP; RRID:AB_2118685
Anti-Nqo1 antibody	Proteintech	Cat# 11451-1-AP; RRID:AB_2298729
Anti-Gclc antibody	ABclonal	Cat# A1038; RRID:AB_2757927
Anti-Gclm antibody	ABclonal	Cat# A13989; RRID:AB_2760843
Anti-Odc1 antibody	ABclonal	Cat# A1948; RRID:AB_2763974
Anti-β-Actin antibody	ABclonal	Cat# AC004; RRID:AB_2737399
HRP Goat Anti-Rabbit IgG (H+L)	ABclonal	Cat# AS014; RRID:AB_2769854
HRP Mouse Anti-Rabbit IgG Light Chain	ABclonal	Cat# AS061; RRID:AB_2864055
Chemicals, peptides, and recombinant proteins		
Recombinant mouse M-CSF protein	Sino Biological	Cat# 51112-MNAH
Recombinant mouse RANK L/TNFSF11	R&D Systems	Cat# 462-TEC
Bitopertin	Selleck	Cat# S8219
Deferoxamine	Selleck	Cat# S5742
Eflornithine	Selleck	Cat# S4582
L-ornithine	MedChemExpress	Cat# 17437
Zoledronic acid	MedChemExpress	Cat# HY13777A
Calcein	Sigma	Cat# C0875
Alizarin Red S Solution	Oricell	Cat# ALIR-10001
Alizarin Complexone	Sigma-Aldrich	Cat# A3882
Mouse food	Experimental Animal Center of Tongji Hospital	Cat #230010367
Critical commercial assays		
Iron Assay Kit (Colorimetric)	Abcam	Cat# ab83366
Ornithine Assay Kit (Fluorometric)	Abcam	Cat# ab252903
Mouse CTX ELISA kit	Bangyi Biotechnology	Cat# BYE30118
Mouse P1NP ELISA kit	Bangyi Biotechnology	Cat# BYE30834
Alkaline phosphatase stain Kit	Beyotime	Cat# C3206
TRAP staining kit	Sigma-Aldrich	NA
ChIP assay kit	Beyotime	Cat# P2078
Protein A/G magnetic beads	MedChemExpress	Cat# HY-K0202A
Immunoprecipitation assay buffer	Beyotime	Cat# P0013
Deposited data		
Raw Data	This paper	Data S1
Transcriptomics and metabolomics data	Mendeley.com	Mendeley Data, https://doi.org/10.17632/4kc5dn9ftm.1

(*Continued on next page*)

Please cite this article in press as: Dong et al., A clinical-stage Nrf2 activator suppresses osteoclast differentiation via the iron-ornithine axis, Cell Metabolism (2024), https://doi.org/10.1016/j.cmet.2024.03.005

Continued

REAGENT or RESOURCE	SOURCE	IDENTIFIER
Experimental models: Cell lines		
Mouse: MC3T3-E1 cell line	Pricella	Cat# CL-0378
Human: HEK-293T cell line	Pricella	Cat# CL-0005
Experimental models: Organisms/strains		
Mouse: C57BL/6 (Wt) mice	Vital River	N/A
Mouse: C57BL/6 (Nrf2-KO) mice	Prof. Peng Zhang	Wuhan University
Oligonucleotides		
Primers for Ctsk, see Table S2	Icongene	N/A
Primers for Mmp9, see Table S2	Icongene	N/A
Primers for Trap, see Table S2	Icongene	N/A
Primers for Odc1, see Table S2	Icongene	N/A
Primers for Slc40a1, see Table S2	Icongene	N/A
Primers for Gclc, see Table S2	Icongene	N/A
Primers for Gclm, see Table S2	Icongene	N/A
Primers for Nqo1, see Table S2	Icongene	N/A
Primers for Nfe2l2, see Table S2	Icongene	N/A
ShRNA sequence targeting mouse *Slc40a1*, see Table S3	ViGene Biosciences	N/A
Recombinant DNA		
Adenovirus for shRNA delivery	ViGene Biosciences	Cat# 20220106004
Plasmid: pADM-mCMV-copGFP	ViGene Biosciences	Cat# pAD100014-KD
Plasmid: PGL3-basic	This paper	N/A
Plasmid: pRL-TK	This paper	N/A
Software and algorithms		
Osteomeasure	OsteoMetrics	Core facility of Biomedical, Xiamen University
R software (4.1.3)	R Software Foundation	https://www.r-project.org/
ImageJ software	N/A	https://imagej.nih.gov/ij/
Micro-CT system	Scanco Medical	N/A
STRING database	N/A	https://www.string-db.org/
MetaboAnalyst	N/A	https://www.metaboanalyst.ca/home.xhtml
Biacore T200 Evaluation Software	Cytiva	N/A
UK Biobank data	UK Biobank Board	https://www.ukbiobank.ac.uk/
Other		
Biacore T200 system	Cytiva	N/A

RESOURCE AVAILABILITY

Lead contact

Further information and requests for resources and reagents should be directed to and will be fulfilled by the lead contact, Kehan Song (kehansong@tjh.tjmu.edu.cn).

Materials availability

All the materials used in this study were either commercially purchased or gifted via cooperation. No new reagents were generated in this study.

Data and code availability

- The full-length, unprocessed western blots were provided in a PDF file. The primary values that were used to create all the graphs in the paper were indicated in an Excel file. The two files were combined into Data S1 in the supplementary files. The UK Biobank data used in this article can be requested from the corresponding authors for academic aims.
- No new code was generated in this study.
- Any additional information required to reanalyze the data reported in this paper is available from the lead contact upon request.

Please cite this article in press as: Dong et al., A clinical-stage Nrf2 activator suppresses osteoclast differentiation via the iron-ornithine axis, Cell Metabolism (2024), https://doi.org/10.1016/j.cmet.2024.03.005

EXPERIMENTAL MODEL AND SUBJECT DETAILS

UK Biobank data

Data from the UK Biobank (Application ID: 81888) were used to explore the association between iron overload and osteoporosis risk. The UK Biobank is a population-based prospective study of the influence of lifestyle and genetic factors on disease risk. The UK Biobank recruited over 0.5 million people aged 50 to 70 from the UK over a five-year period between 2006 and 2010. Each participant gave informed written consent, completed a comprehensive lifestyle and exposure questionnaire, and underwent biological sample testing and radiological examinations. All information was followed up from the date of initial recruitment. In this study, we used the genome sequencing data from UK Biobank participants to investigate the association between single nucleotide polymorphisms (SNPs) and BMD. We also used the clinical data to investigate the association between iron overload and the risk of developing osteoporosis. Cases of osteoporosis were identified using ICD 10 codes (Table S1).

Mouse model

$Nrf2^{-/-}$ mice generated by CRISPR-Cas9 technology were gifted by Prof. Peng Zhang of Wuhan University. All the animal studies and procedures were approved by the Animal Care and Use Committee of our institution. Mice were housed under 25°C in specific-pathogen-free rooms with free access to water and food. Mouse food was provided by the Experimental Animal Center of Tongji Hospital (#230010367). Mice were subjected to ovariectomy (OVX) at 12 weeks of age, as described in detail in our previous study.[47] Drug treatment was initiated one week after OVX. For bitopertin treatment, wildtype mice were randomly divided into sham, OVX, OVX + bitopertin (6 mg/kg) and OVX + bitopertin (30 mg/kg) groups (n=6 for each group). Bitopertin was dissolved in dimethyl sulfoxide and further diluted in ddH_2O containing 0.03% Tween 80, as introduced in a previous pharmacokinetic study of the drug.[48] Bitopertin was administered via oral gavage five days a week for six weeks.

Glycine was administered via drinking water for six weeks. The doses of glycine in mice were translated from the doses of glycine in human clinical trials, according to the body surface area normalization methods.[22] Briefly, the clinical trial dose of glycine was 0.8 g/kg in human subjects,[49,50] and the mouse equivalent dose was 10 g/kg based on body surface area normalization. We assumed that a 0.02-kg mouse drinks 8 mL water per day, and the glycine concentration in the drinking water was calculated as 2.5%. This concentration of glycine was further reduced to 0.5% as the low glycine supplementation group. Such doses were close to that (1%) in other glycine animal studies published previously.[49,51]

To compare the efficacy and safety of bitopertin, and the other two clinically approved Nrf2 activators, DMF and OMA, and zoledronic acid, we used the mouse equivalent dose of DMF and OMA in clinical trials. The human dose of DMF and OMA in clinical trials was 240 mg twice daily[52] and 150 mg per day,[34] respectively. Using the same dose translation approach as bitopertin, the mouse equivalent dose of DMF and OMA was calculated to be 50 mg/kg twice daily and 30 mg/kg per day. We employed the doses and frequencies of the three activators to compare their efficacy and safety in wild-type OVX mice. Zoledronic acid (0.05 mg/kg) was given only once as positive control during the entire course of treatment.

For drug treatments in $Nrf2^{-/-}$ mice, the doses of bitopertin, deferoxamine (DFO), and eflornithine were 6 mg/kg, 30 mg/kg, and 500 mg/kg, respectively, according to previous studies.[53,54] DFO and eflornithine were administered via intraperitoneal injection, and the frequencies and courses of administration of the two drugs were the same as that for bitopertin in wildtype mice.

Cell culture

Osteoclast differentiation, TRAP staining, and bone resorptive assay

Osteoclast differentiation was induced from BMDMs obtained from the bone marrow of bilateral femurs and tibias of 8-week-old mice. Bone marrow cells were diluted and cultured in alpha-modified Eagle's medium (α-MEM; BOSTER Bio; Wuhan, China) containing 30 ng/mL MCSF in 10-cm dishes for 16 h. The supernatants were then transferred to a new 10-cm dish. BMDMs adhering to the bottom were used for subsequent experiments. To induce osteoclast differentiation, BMDMs were seeded on 96-well plates at 2×10^4 cells per well. Osteoclast differentiation was induced in α-MEM in the presence of 30 ng/mL MCSF and 100 ng/mL RANKL for 5 days. Osteoclasts were then washed with PBS, fixed in paraformaldehyde (4%) for 15 minutes, and washed again with ddH2O. TRAP staining was performed with the TRAP staining kit (Sigma Aldrich). After staining, multinucleated cells were counted as osteoclasts and the images were taken under a microscope. The bone resorption assay was performed on hydroxyapatite-coated Osteo Assay strip well plates (Corning, USA). After five days of osteoclast induction, cells were lysed and the hydroxyapatite surface was photographed under a microscope. The resorption area was measured using Image J software.

Osteoblast differentiation, ALP staining, and mineralization assay

Osteoblast differentiation was induced using MC3T3 cells in α-MEM supplemented with b-glycerophosphate (10 mM), ascorbic acid (50 μg/mL), and dexamethasone (10 nM). After seven days of osteoblast induction, ALP staining assay was performed according to the instructions of the alkaline phosphatase staining kit (#C3206, Beyotime, Beijing, China). Alizarin red S staining was performed 21 days after osteogenic induction to evaluate the mineralization status. After seven days of induction, we also harvested cells and extracted total RNA to evaluate the mRNA expression of osteoblast-related genes.

Please cite this article in press as: Dong et al., A clinical-stage Nrf2 activator suppresses osteoclast differentiation via the iron-ornithine axis, Cell Metabolism (2024), https://doi.org/10.1016/j.cmet.2024.03.005

METHOD DETAILS

Detection of bone mineral apposition rate

We performed calcein and alizarin red deposition experiment to evaluate the effects of bitopertin on mineral apposition of bone. Briefly, Calcein (#C0875, sigma; 5mg/ml) was administrated to mice via intraperitoneally injection 7 days before sacrifice, followed by alizarin red (#A3882, sigma; 0.015g/ml) intraperitoneally injection 2 days before sacrifice. The femora of each mouse were harvested after sacrifice and were fixed in 4% paraformaldehyde for one day, dehydrated by 30 percent sucrose for 3 days, followed by embedding in O.C.T. Compound. Femur sections were obtained with a freezing microtome and the representative images of the calcein and alizarin red deposition bands were obtained in a fluorescence microscope. The distance between the deposition bands were measured by ImageJ software and the mineral apposition rate was calculated as the mean apposition distance (μM) per day.

Micro-computed tomography (μCT) analysis

After the in vivo interventions, the mice were sacrificed and the bilateral femurs of each experimental mouse were collected and fixed in 4% paraformaldehyde. The left femurs were scanned in the μCT system (Scanco Medical) for bone morphological analysis. Scanning parameters were set at 100 kV and 98 μA, with a resolution of 10 per pixel. Trabecular parameters included bone volume/tissue volume (BV/TV), trabecular number (Tb.N), trabecular space (Tb.Sp), and trabecular thickness (Tb.Th). Cortical parameters included cortical area (Ct.Ar), total area (Tt.Ar), Ct.Ar/Tt.Ar, and cortical thickness (Ct.Th). The built-in software of the μCT was used for bone parameter analysis and three-dimensional reconstruction.

Histomorphometry analysis

The right femur of each mouse was decalcified in 10% EDTA solution for 2 weeks. The femurs were then embedded in paraffin and were sectioned at 5μm thickness. Osteoclast formation was evaluated by TRAP staining and osteoblast formation was evaluated by toluidine blue and fast green staining. Images of the areas of interest on the stained sections were taken at the same regions of each femur slice. Histomorphometric parameters, including osteoclast number per bone perimeter (N.Oc/B.Pm), osteoclast surface (Oc.S/BS), osteoblast number per bone perimeter (N.Ob/ B.Pm), and osteoblast surface per bone surface (Ob.S/BS), were analyzed in the Osteomeasure Analysis System (Osteometrics). All analysis was performed according to the recommendation of the Nomenclature Committee of the American Society for Bone and Mineral Research.[55]

Immunofluorescence staining

Immunofluorescence staining was performed on the paraffin-embedded femur sections after dewaxing. Before staining, the femur sections were blocked with 5% BSA solution for 30 min. Subsequently, the blocking solution was removed and the sections were incubated with the primary antibodies at 4 °C overnight. On the next day, the femur sections were washed for three times, followed by incubation with the second fluorescent antibody of the same origin to the primary antibody in darkroom for 1 h. The nuclei were stained with DAPI solution at room temperature for 10 min. All the imagines were obtained under a fluorescence microscopy (#80i, Nikon, Japan). The primary antibodies used for immunofluorescence staining were as follows: Nrf2 (#16396-1-AP, Proteintech Group, Wuhan, China); CTSK (#sc-48353, Santa Cruz Biotechnology").

Enzyme-linked immunosorbent assay (ELISA)

CTX and P1NP were used as the serum markers of osteoclastic bone resorption and osteoblastic bone formation, respectively. We used ELISA assay kits of CTX (Bangyi Biotechnology, Shanghai, China) and P1NP (Bangyi Biotechnology, Shanghai, China) to detect the serum levels of the two markers. Blood samples were collected from the orbital venous plexus of each experimental mouse. The serum was collected after centrifugation of the blood samples under 4°C at 2000 rpm for 30 min, and was used for ELISA assay according to the manufacturer's instructions.

Mouse blood biochemistry assay

Blood biochemistry assay was performed at Servicebio (Wuhan, China) to evaluate the influence of bitopertin and other Nrf2 activators on organ function or injury. Blood samples were prepared the same as that used in ELISA assay. We detected the serum levels of ALT, ASL, and albumin as markers of liver function; blood urea nitrogen (BUN) and creatinine as markers of kidney function; creatine kinase and Creatine Kinase MB (CK-MB) as markers of myocardial damage.

RNA sequencing and metabolomics assay

The BMDMs from wildtype or $Nrf2^{-/-}$ mice were used for RNA sequencing and metabolomics assay. For RNA sequencing, BMDMs were seeded on 6-well plates with 1×10^6 cells per well. Each group had four or five replicates from different mice and cells were collected after three days of culture and intervention. Total RNA was extracted with TRIzol (Takara, Japan). For the metabolomic assay, BMDMs were cultured in 10-cm dishes with 1×10^7 cells per dish. After intervention, cells were collected in prechilled 80% methanol and were subjected to three freeze-thaw cycles in liquid nitrogen. LC-MS/MS was used for the untargeted metabolomic assay. All assays were performed by Novogene (Beijing, China).

Please cite this article in press as: Dong et al., A clinical-stage Nrf2 activator suppresses osteoclast differentiation via the iron-ornithine axis, Cell Metabolism (2024), https://doi.org/10.1016/j.cmet.2024.03.005

Bioinformatic analysis

RNA sequencing data were analyzed using R software (version 4.1.3). We identified differentially expressed genes (DEGs) by setting the threshold of $|\log_2 Foldchange|$ as 0.5 and the P value as 0.05. Kyoto Encyclopedia of Genes and Genomes (KEGG) analysis was then performed to determine significantly enriched pathways of the DEGs. Protein-protein interaction (PPI) networks of the DEGs were constructed in the STRING database: https://www.string-db.org/. The PPI networks were then subjected to Cytoscape software. Then, the top 10 hub genes of the PPI network were determined by the Maximal Clique Centrality (MCC) algorithm in the CytoHubba plugin of the software. In addition, we also performed GSEA for two-group sequencing and gene set variation analysis (GSVA) analysis for three-group sequencing to investigate the changes in the pathways of interest.

The analysis of the metabolomics data was performed in the MetaboAnalyst platform (V5.0): https://www.metaboanalyst.ca/. In the platform, the statistical analysis module was used for principal component analysis (PCA) and fold-change calculation. In this module, the orthogonal Partial Least Squares - Discriminant Analysis (orthoPLS-DA) model was used to calculate variable importance in projection (VIP). We used VIP > 1, $|\log_2(\text{fold change})| > 0.5$, and $P < 0.05$ as benchmarks to screen for differential metabolites. Finally, we analyzed the involved pathway of the identified differential metabolites in the enrichment analysis module.

Single-cell RNA-sequencing data processing and analysis

We obtained single-cell RNA-sequencing data of bone tissue from osteoporosis patients (GEO: GSM4423510)[56] and healthy controls (GEO: GSE169396)[57] from the Gene Expression Omnibus (GEO) database. Data from different samples were integrated using the Seurat package and batch effects were adjusted using the Harmony package in R software. For data analysis, the Seurat package was used to perform nonlinear dimensional reduction. A total of 2500 highly variable genes were selected for principal component analysis. The functions RunUMAP and FindClusters were used to select principal components. The FindAllMarkers function was used to identify differential expression genes (DEGs) and the ggplot2 package was used for plotting. Osteoclasts in the bone marrow differentiate from the myeloid lineage of bone marrow cells that include common myeloid progenitor (CMP), monocytes and macrophages. We defined c-Fms$^+$ monocytes and c-Fms$^+$ macrophages as osteoclast precursors that express c-Fms in the plasma surface and possess the ability to differentiate into mature osteoclasts. The cell ratio of osteoclast precursors in the control and disease group and the expression of NFE2L2 and SLC40A1 in this cell population were analyzed.

Molecular docking

The three-dimensional (3D) crystal structure file of Keap1 (PDB: 7OFE) was downloaded from the RCSB Protein Data Bank database: https://www.rcsb.org/, while the structure file of bitopertin (ZINC: ZINC53294263) was downloaded from the ZINC database. Molecular docking of the two structures was performed in Autodock software (version 1.5.7) after addition of hydrogen atoms and removal of water molecules. The binding energy of the two molecules was then calculated in Autodock to evaluate the binding affinity. The 3D model diagram of Keap1-bitopertin binding was generated in the PyMoL software, while the 2D-diagram was generated in the Maestro software (version 13.5). We calculated the binding free energy of Keap1-bitopertin in Autodock to evaluate the docking performance between the two molecules. In general, a binding energy of less than -7.0 kcal/mol indicates a very good binding affinity.

Surface plasmon resonance (SPR) analysis

SPR analysis was run on a Biacore T200 system (Cytiva) with a Series S Sensor Chip CM5. Briefly, the ligand (Keap1 protein, Keap1 Kelch domain, Keap1 BTB domain, or Keap1 Back domain) was immobilized to the CM5 Chip via covalent bonds to the amino acid residues in immobilization buffer. Subsequently, different concentrations of bitopertin were diluted in the analyte buffer and were injected into the flowing channel to allow interaction between Keap1 and bitopertin. The interacting phase included 120 s of association phase and 300 s of dissociation phase. The data were analyzed in a Biacore T200 Evaluation Software (Cytiva).

Dual luciferase reporter assay

The regulation of Nrf2 on *Slc40a1* transcription was evaluated by dual luciferase reporter assay. we constructed three luciferase reporter vectors containing the wildtype promoter, the binding site 1 mutated promoter, and the binding site 2 mutated promoter of the *Slc40a1* gene. These promoters were constructed into the pGL3-basic plasmids. To create the mutant *Slc40a1* promoter constructs, the first predicted Nrf2 binding site CTGACTTAGCC was mutated to AGTCAGGCTAA, while the second predicted binding site GTGTCTCAGCA was mutated to TGTGAGACTAC. The *Slc40a1* promoter plasmids were then co-transfected with human Nrf2-overexpressing plasmids and pRL-TK plasmids into HEK-293T cells. After 48 hours of incubation, the cells were lysed and assayed for luciferase activity. Firefly luciferase activity was normalized to Renilla luciferase activity for the final analysis.

Chromatin immunoprecipitation and PCR (ChIP-qPCR) assay

ChIP assay was performed by using a ChIP assay kit (#P2078, Beyotime, Beijing, China). Detailed procedures were performed according to the manufacturer's instructions. The Nrf2 antibody used for immunoprecipitation in this assay was obtained from Proteintech (#16396-1-AP, Wuhan, China). The PCR assay was performed by using the following primers of human *SLC40A1* gene (F, TCTACGGGAAGTAATTTT; R, GGTAAATAAACCCCTCCACT). The PCR products were detected by electrophoresis with 2% agarose gel.

Please cite this article in press as: Dong et al., A clinical-stage Nrf2 activator suppresses osteoclast differentiation via the iron-ornithine axis, Cell Metabolism (2024), https://doi.org/10.1016/j.cmet.2024.03.005

Measurement of intracellular iron and ornithine

Intracellular iron and ornithine levels were measured using the Iron Assay Kit (Colorimetric; # ab83366, Abcam) and Ornithine Assay Kit (Fluorometric; #ab252903, Abcam), respectively. For sample preparation, BMDMs were cultured on 10-cm dishes and were subjected to various interventions. After three days, cells were harvested with cell scrapers and the total number of harvested cells was counted. The cells were then washed with ice-cold PBS for three times and lysed in 100 μL iron or ornithine assay buffer. The following procedures were performed according to the instructions of the two assay kits to obtain the final concentration of iron or ornithine in the 100 μL buffer. For data analysis, we calculated the absolute content of ornithine or iron in the harvested cells. The final amount of iron or ornithine was presented as that per 1×10^6 cells to compare their differences.

Real-time quantitative PCR (RT-qPCR)

Total RNA was extracted from cell samples using TRIzol reagent (Takara, Japan) as previously described.[47] The final RNA sample was dissolved in ddH2O, and a total of 1 μg RNA from each group was reverse transcribed into cDNA in a volume of 20 μL by using the HiScript III All-in-one RT SuperMix Perfect for qPCR (Vazyme Biotech, Nanjing, China). RT-qPCR was then performed to detect the cDNA of target genes by using the HiScript II Q RT SuperMix for qPCR (Vazyme Biotech, Nanjing, China). The forward and reverse PCR primers are listed in Table S2. For data analysis, the expression of the target genes was normalized to that of β-actin.

Western blot assay

Total proteins were extracted from cell samples by using the RIPA buffer containing 1 % proteinase inhibitor and 1% phosphotransferase inhibitor. The samples were then sonicated and centrifuged at 12,000 rpm for 30 minutes. The supernatants were collected and the protein concentration was measured using the bicinchoninic acid (BCA) kit (Boster Biotechnology, Wuhan, China). For Western blotting, proteins were separated in SDS-PAGE by electrophoresis (80V) and transferred to PVDF membranes (#IPVH00010, Millipore, Boston, USA). The membranes were then blocked in 5% BSA dissolved in TBS (with 0.1 % Tween 20) for 1 hour at room temperature and incubated with primary antibodies overnight at 4°C. The next day, the membranes were washed for three times and incubated with the secondary antibodies for 1hour. The final protein bands were detected with ECL solution (Yeasen, Shanghai, China) and analyzed using the ChemiDoc XRS system (BioRad, California, USA).

Protein-protein interaction and Nrf2 ubiquitination assay

To detect the interaction between Nrf2 and Keap1 and Nrf2 ubiquitination, cells were cultured on 10-cm dishes with or without bitopertin treatment for 48 hours. The cells were then treated with MG132 (10 μM) for 4 hours, washed with pre-chilled PBS, and lysed in the immunoprecipitation (IP) assay buffer (Beyotime Biotechnology, Beijing, China). After centrifugation, the total protein content in the lysates was quantified, and 500 μg of protein in the lysates was incubated with the Protein A/G magnetic beads (#HY-K0202A, MedChemExpress) for 2 hours at 4°C. The beads were pre-washed and incubated with primary Nrf2 antibody (2 μg) for 2 hours at 4°C. The antigen-antibody-bead complex was then washed five times with IP buffer, resuspended in 1× SDS loading buffer, and boiled at 95°C for 5 minutes. Samples in the SDS loading buffer were further subjected to Western blot analysis.

Adenovirus transfection

Adenovirus-mediated shRNA interference was used to knock down the expression of *Slc40a1* in BMDMs. Four shRNAs targeting the *Slc40a1* mRNA were constructed in an adeno vector (ViGene Biosciences, Shandong, China). The sequence of each shRNA is shown in Table S3. Scramble sequences of the same length were incorporated into the same type of vector as the control group. For adenovirus transfection, cells were incubated with *Slc40a1* adenovirus or control adenovirus for 12 hours at a multiplicity of infection (MOI) of 200 per cell. The medium was then removed and the cells were cultured for another two days before various interventions or treatments. Knockdown efficiencies were determined by Western blot.

QUANTIFICATION AND STATISTICAL ANALYSIS

Data from the current study were analyzed using GraphPad Prim 7. Each experiment was performed in three independent replicates. Data were expressed as mean ± SEM (standard error of mean) for each group. Unpaired Student t-test was used to compare differences between two groups, while one-way or two-way ANOVA followed by Bonferroni multiple comparison test was used to compare differences among three or more groups. The sample sizes of animal study and the replicates of cell experiments in each statistical analysis are indicated in the figure legends. In all statistical tests, a P-value less than 0.05 was considered as statistically significant.